Validation of a New and Cost Effective Technique to Estimate Reservoir Pressure and Permeability in Low-Permeability Reservoirs

A Thesis

Presented to

the Faculty of the Department of Petroleum Engineering

University of Houston

In Partial Fulfillment

of the Requirements for the Degree

Master of Science

in Petroleum Engineering

by

ZOHA NASIZADEH

December 2014

Validation of a New and Cost Effective Technique to Estimate Reservoir Pressure and Permeability in Low-Permeability Reservoirs

Zoha Nasizadeh

Approved:

Chair of the Committee
Dr. W. John Lee,
Hugh Roy and Lillie Cranz Cullen
Distinguished University Chair
Professor
Petroleum Engineering

Committee Members:

John Adams,
Unconventional Resource COP Leader
and Advisor
BP America Inc.

Dr. Arthur Weglein,
Hugh Roy and Lillie-Cranz Cullen
Distinguished Professor
Dept. of Physics
Dept. of Geosciences, Reflection
Seismology

Dr. Suresh Khator,
Associate Dean
Cullen College of Engineering

Dr. Thomas K. Holley,
Professor and Director
Petroleum Engineering

Acknowledgements

I would like to express my special appreciation and thanks to my advisor, Dr. John Lee, for his invaluable advices and guidance throughout this project. He was always supportive, encouraging and willing to share his ever more fascinating ideas which were crucial to the success of this work.

I would like to thank John Adams and Bryan Dotson for their guidance and support through my research. They provided several field data which were critical part of this research. I am especially grateful to my committee members, Dr. Arthur Weglein, and John Adams for their sound advices and inputs towards the completion of this work.

I would like to thank Dr. Thomas Holly, Ms. Anne Sturm, and all professors in Petroleum Engineering Department at the University of Houston for providing opportunities and resources to complete this research work.

A special thanks to my family and friends. Words cannot express how grateful I am to my mother and father, Parvin and Ehsan for all of the sacrifices they have made for me. Similarly, I am grateful to my parents in law for their emotional encouragements. I am thankful to my lovely sister and brothers who motivated me through all stages of my education. I would also like to thank all of my friends for their good company and their assistance during this work.

Last but not least, I would like to express my deepest appreciation to my beloved husband, Rohollah who have supported me in every possible way. My achievements would have not been possible without his help and inspiration. To whom I dedicate this thesis.

Validation of a New and Cost Effective Technique to Estimate Reservoir Pressure and Permeability in Low-Permeability Reservoirs

An Abstract

of a

Thesis

Presented to

the Faculty of the Department of Petroleum Engineering

University of Houston

In Partial Fulfillment

of the Requirements for the Degree

Master of Science

in Petroleum Engineering

by

ZOHA NASIZADEH

December 2014

Abstract

I developed the mathematical basis for a new and cost effective method to estimate reservoir pressure and effective water permeability in low permeability reservoirs. This method, called Baseline/Calibration, was successfully tested in Wamsutter fields. This approach, which is an alternative to time-consuming DFIT tests and conventional pressure buildup tests, requires injection of water in multiple short stages. Sandface pressure and flow rate are analyzed to estimate reservoir pressure and permeability.

I derived analytical expressions which provide a mathematical basis for this method. The analytical formulations are based on transient solutions to the diffusivity equation, the principle of superposition, and assume piston-like displacement of reservoir fluids with injected water.

I constructed several numerical simulation models and validated the proposed technique. I also analyzed flow rate and pressure data from two field trials performed in the Almond formation of the Wamsutter field. The results of numerical simulation and field trials of this method verified that our method accurately determines reservoir pressure with short injection tests.

Reservoir pressure is a fundamental property of the reservoir and its depletion provides an insight in to the reservoir dynamics and drainage pattern. Measurements of formation pressure and in-situ reservoir permeability are important for a variety of reasons including estimation of ultimate recovery, production forecasting, and optimization of depletion planning.

Unconventional gas reservoirs are economically viable hydrocarbon prospects that have proven to be very successful. However, conventional well tests methods are often impractical in unconventional reservoirs. Long shut-in times are required for estimates of reservoir pressure and reservoir permeability.

Table of Contents

List of Figures

List of Tables

Nomenclature

Variables

A = Reservoir area, ft^2

B_w = Formation volume factor of water, RB/STB

c_f = Formation compressibility, 1/psi

c_g = Gas compressibility, 1/psi

c_o = Oil compressibility, 1/psi

c_t = Total reservoir compressibility, 1/psi

c_w = Water compressibility, 1/psi

Ei = Exponential integral function, dimensionless

h = Reservoir height, ft

k = Formation Permeability, mD

k_{eg} = Effective gas permeability, mD

k_{ew} = Effective water permeability, mD

$k_f w_f$ = Fracture Conductivity, mD-ft

L_f = Fracture half length, ft

p = Reservoir pressure, psi

$\bar{p}$ = Average pressure of invaded zone, psi

p_0 = Reference pressure, psi

p_D = Dimensionless pressure, dimensionless

p_{bh} = Bottom-hole pressure, psi

p_i = Initial reservoir pressure, psi

p_p = Real gas pseudo-pressure, $\mathrm{psi}^2/\mathrm{cp}$

p_{trans} = Transient pressure gradient, psi

p_{ww} = Steady state pressure gradient, psi

q = Flow rate, STB/d

Q = Cumulative injected water, bbl

r = Radius of investigation, ft

r_D = Dimensionless radius, dimensionless

r_e = Radius of invasion, ft

r_w = Wellbore radius, ft

S_{gr} = Residual gas saturation, dimensionless

S_{wi} = Initial water saturation, dimensionless

t_D = Dimensionless time, dimensionless

t_i = Time at i^{th} injection or shut-in time, hour

t_p = injection time, hour

T = Temperature, $^\circ\mathrm{R}$

u_r = Volumetric flow rate in radial direction, $\mathrm{RB/Dft}^2$

V = Injected volume, bbl

Δt = shut-in time, hour

λ_g = Gas mobility, mD/cp

λ_t = Total mobility, mD/cp

λ_w = Water mobility, mD/cp

μ = Viscosity, cp

μ_g = Viscosity of gas phase, cp

μ_o = Viscosity of oil phase, cp

μ_w = Viscosity of water phase, cp

ρ = Fluid density, $\mathrm{lbm/ft^3}$

ρ_0 = Density at $\mathrm{p_0}$, $\mathrm{lbm/ft^3}$

ϕ = Reservoir porosity, dimensionless

Chapter 1

Introduction

Unconventional gas reservoirs are economically viable hydrocarbon prospect that have proven to be very successful in the United States. More than fifty percent of the currently identified gas resources in the United States are unconventional (Adams et al., 2012). This research is guided towards exploring methods to estimate formation pressure in unconventional reservoirs.

In this chapter, I describe the problem and motivation for developing a new method for estimation of formation pressure and permeability in unconventional reservoirs. I present a review of literature for existing methods and mathematical formulations to estimate formation pressure and permeability, a list of objectives, and a brief review of all chapters included in this thesis.

1.1 Problem Statement

Pressure is a fundamental property of a reservoir and its depletion provides an insight into the reservoir dynamics and drainage pattern. Understanding the reservoir depletion behavior is necessary in optimizing field development. Estimation of reservoir properties such as formation pressure, in-situ reservoir permeability, and closure pressure is important for variety of reasons including estimation of ultimate recovery, production forecasting, and optimization of depletion planning (Adams et al., 2012). Furthermore, completion

designs, modeling studies, and future field development decisions are all improved with better knowledge of current and historical reservoir pressures (Adams et al., 2013).

Performing conventional transient tests is practically challenging in unconventional gas reservoirs because the formation permeability is very low in unconventional gas reservoirs. Even though well-known conventional well testing methods are applicable in unconventional reservoirs, however, they are often impractical because of long shut-in time (Jin et al., 2013). There is lack of a practical method to estimate formation pressure and permeability in a cost effective way.

1.2 Literature Review

Several methods are currently in use to obtain formation pressure and permeability in tight gas reservoirs. The most popular method to estimate formation properties in unconventional reservoirs is Diagnostic Fracture Injection Test (DFIT). In this section, I briefly review the main structure of DFIT, different types of analysis, and advantages and disadvantages of this method.

1.2.1 Diagnostic Fracture Injection Test in Unconventional Reservoirs

The diagnostic fracture injection test (DFIT) or minifrac test is an invaluable tool to evaluate reservoir properties and geomechanical characteristics in unconventional formations. The diagnostic fracture injection test is used to estimate reservoir pore pressure, permeability, and state of stress in the rock strata (Cramer and Nguyen, 2013). This method is conducted before the

main fracturing treatment. DFIT is a process in which the fracturing fluid is injected at a constant rate and high pressure to propagate a small fracture into the formation. After achieving the formation fracture pressure, surface injection is stopped to evaluate and analyze the declining pressure response. **Figure 1-1** represents a typical diagnostic fracture injection test (Cramer and Nguyen, 2013).

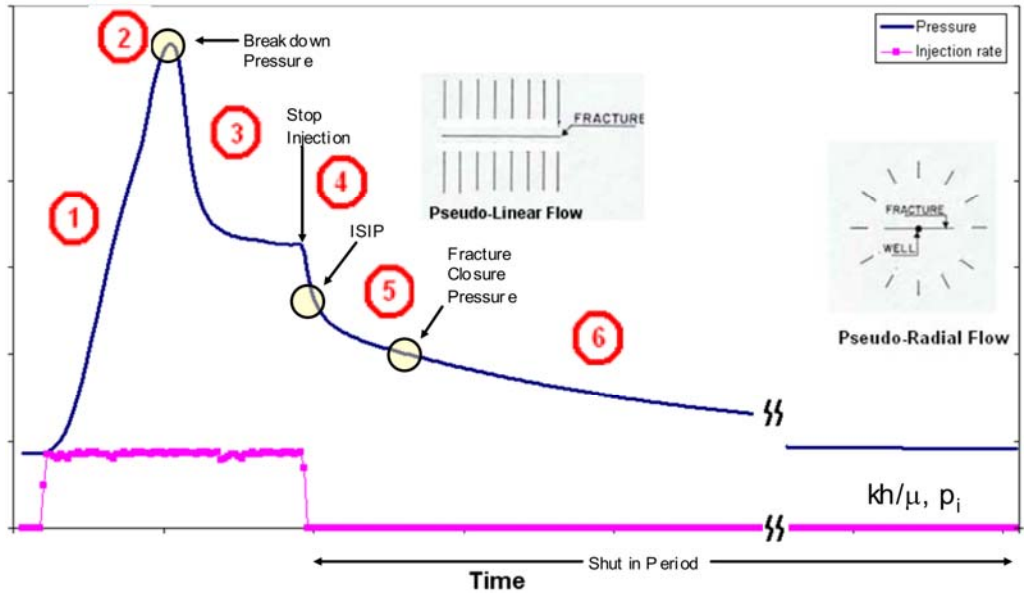

Figure 1-1: Typical diagnostic fracture injection test, injection rate and pressure response (Cramer and Nguyen, 2013).

The following steps are taken during a typical diagnostic fracture injection test (Cramer and Nguyen, 2013):

1) A surface pump is installed to inject water or any other fracturing fluid in to the wellbore and the wellbore fluid is pressurized. The compression time is a function of injection rate, wellbore volume, and formation breakdown pressure.
2) A hydraulic fracture propagates into the reservoir when breakdown pressure is reached.

3) Water injection continues until wellhead pressure becomes stable. This step causes the fracturing fluid to leak off into the formation.
4) Surface injection is stopped and consequently pressure declines rapidly. At this time, an instantaneous shut-in pressure (ISIP) is observed.
5) The shut-in well pressure is recorded and analyzed for signs of fracture closure. Fracture closure pressure is considered to be the same as minimum principal stress.
6) The declining pressure response is evaluated during "after closure period" to observe the signatures of pseudo-linear and pseudo-radial flow regimes.

Before planning a DFIT, it is necessary to define the test objectives. Defining the objectives will help to determine when the test should end and what kind of analysis should be performed (Martin et al., 2013). If the objective is to measure fracture closure pressure, the test can be stopped at the onset of the fracture closure signature from the declining pressure data. Fracture closure pressure could be estimated using "before-closure analysis". If the objective is to evaluate formation transmissibility (kh/μ) and pore pressure (p_i), then DFIT ends at the onset of the observation of signatures corresponding to pseudo-radial, bi-linear, and linear flow regimes. "After-closure" period is evaluated during pseudo-radial, bi-linear, and linear flow regimes. Transmissibility and pore pressure can be derived using pseudo-radial flow solution method, and pore pressure can be obtained from linear flow solution method. In this section, I explain "after-closure analysis" in which we can estimate initial formation pressure and transmissibility.

1.2.2 After-Closure Analysis

After-closure analysis is based on a conventional well test technique called short-term formulation. However, it has been shown that this technique is valid for after-closure data of a diagnostic fracture injection test (Soliman et al., 2005). The majority of conventional well test methods and diagnostic test method are characterized by very short injection or production time followed by a relatively long shut-in time. In the short-term test technique, the principle of superposition is not used to drive the solution for a buildup test. Instead, the coupled flow rate and drawdown/buildup test are solved directly (Soliman, 1986).

If a DIFT is considered as an injection/shut-in test with similarity to the regular injection falloff test, the short-term formulation could be used to analyze the declining pressure data (Soliman et al., 2005). A DFIT is not the same as injection falloff test due to induced fracture during pumping period. At the presence of induced fracture short-term test technique should not be used for “after closure analysis”. However, due to shortness of injection time, the short-term test formulation may be applicable to the declining DFIT pressure with high degree of accuracy (Soliman and Kabir, 2012).

The flow regime reached after sufficient amount of shut-in time depends on the properties of reservoir, fluid, and fracture closure. Here, I present how the method of short-term formulation can be applied to find initial reservoir pressure and transmissibility from different flow regimes including pseudo-radial, linear, and bi-linear flow regimes.

1.2.3 Pseudo-Radial Flow Regime

The pseudo-radial flow regime is reached when the far field area affected by flow is circular. Reaching this flow regime requires the propagated fracture to be fairly short, formation permeability to be relatively high, and formation compressibility to be low. In other words, it is expected to observe pseudo-radial flow regime more in liquid reservoirs than in tighter gas reservoirs (Soliman et al., 2005).

The behavior of the declining pressure data during pseudo-radial flow regime is shown in Equation (1-1). The presence of pseudo-radial flow regime indicates that either the fracture is very short or it is completely closed with little or no residual conductivity. Equations (1-2) and (1-3) are the specialized log-log and derivative forms of Equation (1-1), respectively, and are expressed as

$$p - p_i = \frac{1694.4\, V\mu}{kh} \frac{1}{\left(t_p + \Delta t\right)}, \tag{1-1}$$

$$\log\ (p - p_i) = \log\left(\frac{1694.4\, V\mu}{kh}\right) - \log\left(t_p + \Delta t\right)\ , \text{and} \tag{1-2}$$

$$\log\left(t\frac{\partial p}{\partial t}\right) = \log\left(\frac{1694.4\, V\mu}{kh}\right) - \log\left(t_p + \Delta t\right). \tag{1-3}$$

In Equations (1-1) through (1-3), p and p_i are respectively, the reservoir pressure and initial reservoir pressure in psi. V is the injected volume in bbl, μ is viscosity in cp, k is reservoir permeability in mD, h is reservoir depth in ft, t_p is injection time in hour, and Δt is shut-in time in hour.

Equation (1-2) indicates that if a pseudo-radial flow regime dominates the reservoir behavior, a plot of left hand-side versus total time $\left(t_p + \Delta t\right)$ on a log-log

graph yields a straight line with a slope of -1. Equation (1-3) can be used to diagnose a pseudo-radial flow regime because it is independent of initial reservoir pressure. Therefore, plotting the left-hand side of Equation (1-3) vs. the total time on a log-log graph would result a straight line with a slope equal to -1. Therefore, plotting Equation (1-3) could be used to identify different flow regime. After determining the pseudo-radial flow regime, pressure and time data are plotted according to Equation (1-1) to obtain initial reservoir pressure. Equations (1-1) through (1-3) are used to estimate transmissibility, however, it is recommended to use Equation (1-2) for this purpose (Soliman et al., 2005).

1.2.4 Bi-Linear Flow Regime

The bi-linear flow regime can be observed when the propagated fracture is long or is open with some residual conductivity. The bi-linear flow regime indicates that the pressure drop in the reservoir is controlled by two linear flow systems: (i) a linear flow inside the fracture and (ii) a linear flow inside reservoir and at the vicinity of fracture.

Equation (1-4) describes the behavior of pressure data when bi-linear flow regime is observed. Equations (1-5) and (1-6) are the log-log and derivative forms of Equation (1-4), respectively (Soliman et al., 2005), and are expressed as

$$p - p_i = 264.6 \frac{V}{h} (\mu)^{0.75} \left(\frac{1}{\phi c_t k}\right)^{0.25} \frac{1}{\sqrt{k_f w_f}} \left(\frac{1}{t_p + \Delta t}\right)^{0.75}, \quad (1\text{-}4)$$

$$\log(p - p_i) = \log\left(264.6\frac{V}{h}\,(\mu)^{0.75}\left(\frac{1}{\phi c_t k}\right)^{0.25}\frac{1}{\sqrt{k_f w_f}}\right) - 0.75\log(t_p + \Delta t), \text{and} \qquad (1\text{-}5)$$

$$\log\left(t\frac{\partial p}{\partial t}\right) = \log\left(198.45\,\frac{V}{h}\,(\mu)^{0.75}\left(\frac{1}{\phi c_t k}\right)^{0.25}\frac{1}{\sqrt{k_f w_f}}\right) - 0.75\log(t_p + \Delta t)\,. \qquad (1\text{-}6)$$

In the above equations, ϕ is reservoir porosity, c_t is total reservoir compressibility in $1/psi$, and $k_f w_f$ is fracture conductivity in *mD-ft*. Equation (1-6) can be used for diagnostic plot because it is only a function of observed pressure, total time, and the flow regime. This plot yields a straight line with slope of -0.75 for a bi-linear flow regime. The initial reservoir pressure can be determined using Equation (1-4).

1.2.5 Linear Flow Regime

If the induced fracture is fairly long, and it stays open for a long time with high residual conductivity, a linear flow regime will be observed. Reaching a linear flow regime during a DFIT is rare, but it might happen if the formation permeability is low and the DFIT is conducted using an injection fluid containing proppant (Soliman et al., 2005).

Equation (1-7) describes the behavior of a reservoir pressure when a linear flow regime signature is observed. Equations (1-8) and (1-9) are log-log and derivative forms of Equation (1-7), respectively (Soliman et al., 2005), and are given by

$$p - p_i = 31.05\frac{V}{4h}\left(\frac{\mu}{\phi c_t k L_f^2}\right)^{0.5}\left(\frac{1}{t_p + \Delta t}\right)^{0.5}, \qquad (1\text{-}7)$$

$$\log(p - p_i) = \log\left(31.05\frac{V}{4h}\left(\frac{\mu}{\phi c_t k L_f^2}\right)^{0.5}\right) - o.5\log(t_p + \Delta t), \text{and} \quad (1\text{-}8)$$

$$\log\left(t\frac{\partial p}{\partial t}\right) = \log\left(15.525\ \frac{V}{4h}\left(\frac{\mu}{\phi c_t k L_f^2}\right)^{0.5}\right) - o.5\log(t_p + \Delta t), \quad (1\text{-}9)$$

where L_f is fracture half length in ft.

A diagnostic plot using Equation (1-9) is independent of initial reservoir pressure, and can be used to determine a linear flow regime. This plot will yield a straight line with a slope of -0.5. Equation (1-7) can be applied to determine initial reservoir pressure.

There are several benefits for conducting a diagnostic fracture injection test. Formation geomechanical properties, minimum in-situ stress, and fracture closure pressure can be estimated using “before closure analysis” (Soliman et al., 2013). Moreover, initial reservoir pressure and transmissibility can be determined using “after closure analysis”. However, reaching to a bi-linear or a pseudo-radial flow regime, to find p_i and k, can be very time consuming and costly; it often requires multiple days of shut-in. These long shut-in times are not practical in some cases where it delays the fracture stimulation operations (Adams et al., 2013).

1.3 Research Objective

The main objective of this research is to develop the mathematical basis of a cost effective technique to determine initial reservoir pressure and permeability in unconventional formations by:

- developing an analytical solution for pressure variations during injection/shut-ins,
- validating the developed equation and baseline/calibration method in different types of tight gas sand formation,
- correcting the estimated pressure from supercharging effect, and
- investigating a practical method to calculate formation permeability.

1.4 Review of Chapters

I conducted the following steps to achieve the objectives of this research:

- Constructed several synthetic reservoir simulation case studies to perform sequential steps of baseline/calibration method. The synthetic cases included different petrophysical rock types which are representative of the tight gas sand of Wamsutter field.
- Performed baseline/calibration method to estimate formation pressure and compare with the assumed initial pressure values. This step validated numerically the baseline/calibration method in tight gas sand formations.
- Applied currently developed techniques in pressure transient analysis to estimate pressure and investigated a procedure to calibrate each technique to better estimate formation permeability.
- Applied baseline/calibration technique to estimate formation pressure using field test data.

In **Chapter 2**, I describe the baseline/calibration algorithm as well as the mathematical formulations used in this method. I discuss assumptions, solution

to the diffusivity equation with a line source, the principles of superposition in time, and piston-like displacement of water.

Chapter 3 describes the numerical simulation model, properties of assumed reservoir, properties of reservoir fluid, and relative permeability curves. I present several case studies to validate the developed baseline/calibration method.

I analyze the results of numerical simulations for estimating reservoir pressure and permeability using baseline/calibration method in **Chapter 4**.

Chapter 5 discusses the results of baseline/calibration method on real field data. **Chapter 6** summarizes the conclusions of the thesis.

Chapter 2

Baseline/Calibration Method

2.1 Introduction

The baseline/calibration (B/C) method is a new and cost effective technique to estimate reservoir pressure in unconventional gas reservoirs. Measuring reservoir pressure and formation permeability in low permeability gas reservoirs are difficult with current available practices (Adams et al., 2013). However, performing a B/C test and the subsequent analysis will enable us to estimate formation pressure and permeability in a shorter time and for less cost than other current techniques. In this chapter, I describe the procedure for baseline/calibration technique, subsequent analysis of the test data, and the mathematical formulations for the validity of this algorithm with appropriate assumption.

2.2 Baseline/Calibration Technique

The baseline/calibration method consists of two main parts. The first part consists of injection of water in discrete stages using different number of protocols. The second part is the analysis of the pressure and flow rate recorded from the first part. In the following sections, I show a scheme for plotting pressure and rate data which enables measuring formation pressure (Adams et al., 2013). Later, I developed a method to estimate reservoir permeability using the slope of

plotted curves. The B/C method should be conducted after perforation and before the main stimulation job.

A baseline/Calibration test consists of a series of injection events in different stages. I use sandface pressure and injection rate to generate one or more pairs of trend lines, called baseline and calibration trends. Different test protocols can be used to obtain pressure and rate data. These protocols are constant pressure injection test (CPIT), constant rate injection test (CRIT), and falling fluid level test (FFLT). CPIT consists of injection at a constant bottom-hole pressure followed by a short shut-in time. In this protocol, injection rate is changing during injection stage. CRIT consists of injection at a constant rate while bottom-hole pressure is changing. FFLT consists of injection by changing sandface rate and pressure at the same time.

In this study, I used constant rate injection test protocol to perform my numerical simulations and to derive the analytical solution. Once sandface rate and pressure data are obtained, I plotted calibrated baseline trends based on the mathematical formulations described in the following section.

2.3 Mathematical Principle

Mathematical principle for baseline/calibration method is based on the solution to the diffusivity equation, the principle of superposition in time, and piston-like displacement of reservoir fluid with injected water. I describe each of these concepts in the following sections.

2.3.1 Solution to Diffusivity Equation

The partial differential equation corresponding to the transient pressure response of a single phase flow in a reservoir is obtained by a combination of three physical principles:

1. the principle of mass conservation,
2. Darcy's law , and
3. an equation of state for reservoir fluid.

The mass conservation equation, which is known as continuity equation, is given by,

$$\frac{1}{r}\frac{\partial}{\partial r}(r\rho u_r) = -\frac{\partial}{\partial t}(\phi\rho), \tag{2-1}$$

where r is the radius of investigation, ρ is fluid density, u_r is the volumetric flow rate, ϕ is reservoir porosity, t is time. Dacy's law is expressed as

$$u_r = -\frac{k}{\mu}\frac{\partial p}{\partial r}, \tag{2-2}$$

where k is permeability and μ is fluid viscosity. The equation of state for a slightly compressible fluid is

$$\rho = \rho_0 exp[c(p - p_0)], \tag{2-3}$$

where ρ_0 is the density at the reference pressure p_0 and c is fluid compressibility.

The radial diffusivity equation of a single phase can be obtained by combining Equations (2-1) through (2-3), and is given by (Lee et al., 2003)

$$\frac{\partial^2 p}{\partial r^2} + \frac{1}{r}\frac{\partial p}{\partial r} = \frac{\phi\mu c_t}{k}\frac{\partial p}{\partial t}, \tag{2-4}$$

where c_t is total formation compressibility and is defined as

$$c_t = c + c_f \ . \quad (2\text{-}5)$$

In the above equation, c_f is formation compressibility. Equation (2-4) is based on the following assumptions,

- radial flow,
- laminar flow,
- porous medium has constant compressibility and permeability,
- negligible gravity effects,
- isothermal conditions,
- fluid has small and constant compressibility, and
- compressibility times pressure gradient squared product, $c\left(\frac{\partial p}{\partial r}\right)^2$, is negligible.

The diffusivity equation for fluid flow in a reservoir is a partial differential equation of pressure with respect to both space and time. To solve this equation, an initial condition and two boundary conditions are required.

Initial Condition

It is assumed that the reservoir is initially at a constant and uniform pressure throughout the reservoir given by

$$p(r, t = 0) = p_i \ . \quad (2\text{-}6)$$

Outer-Boundary Condition

An infinite-acting reservoir flow is defined as a reservoir in which the influence of reservoir boundaries is not felt during the time in which pressure and

rate data are analyzed. This is the case when a well is producing at early times and the effect of outer boundaries of reservoir are not seen; i.e., the reservoir acts as if there were no boundaries (Matthews and Russell, 1967).

For an infinite acting reservoir, at infinite distance from the wellbore, the reservoir pressure remains as initial pressure, p_i, for all times (Lee et al., 2003). Equation (2-7) expresses the outer-boundary condition as,

$$p(r \to \infty, t) = p_i. \tag{2-7}$$

Inner-Boundary Condition

If a well produces at a constant sandface rate, flow rate at the wellbore, $r = r_w$, can be described with Darcy's law. Equation (2-8) expresses the inner-boundary condition in oil field unit (Lee et al., 2003) as,

$$\left(r\frac{\partial p}{\partial r}\right)_{(r=r_w)} = \frac{141.2qB\mu}{kh}. \tag{2-8}$$

To solve the diffusivity equation, it is convenient to use dimensionless variables. In oil field units, the dimensionless pressure, time and radius are defined as

$$p_D = \frac{kh(p_i - p(r,t))}{141.2qB\mu}, \tag{2-9}$$

$$t_D = \frac{0.0002637kt}{\phi\mu c_t r_w^2}, \text{and} \tag{2-10}$$

$$\boldsymbol{r_D} = \frac{r}{r_w}. \tag{2-11}$$

Substituting Equations (2-9) through (2-11) into Equation (2-4) yields dimensionless diffusivity equation as

$$\frac{\partial^2 p_D}{\partial r_D^2} + \frac{1}{r_D}\frac{\partial p}{\partial r_D} = \frac{\partial p}{\partial t_D}. \quad (2\text{-}12)$$

Dimensionless initial and boundary conditions are shown in Equations (2-13) through (2-15),

$$p_D\,(r_D, 0) = 0, \quad (2\text{-}13)$$

$$\lim_{r_D \to 0}\left(r_D \frac{\partial p_D}{\partial r_D}\right) = -1, \text{and} \quad (2\text{-}14)$$

$$\lim_{r_D \to \infty} p_D(r_D, t_D) = 0. \quad (2\text{-}15)$$

Equation (2-12) is solved using Laplace transformation (Lee et al., 2003). The line source solution in the form of dimensionless variables is given by

$$p_D(r_D, t_D) = -\frac{1}{2}\, Ei\left(-\frac{r_D^2}{4t_D}\right), \quad (2\text{-}16)$$

where Ei is the exponential integral. The exponential integral is defined as

$$Ei(-x) = -\int_x^\infty \frac{e^{-y}}{y} dy\,. \quad (2\text{-}17)$$

Substituting dimensionless parameters in Equation (2-16), offers the pressure as a function of time and radius as

$$p(r, t) = p_i + \frac{70.6\, qB\mu}{kh}\, Ei\left(-\frac{948\phi\mu c_t r^2}{kt}\right). \quad (2\text{-}18)$$

Lee et al. (2003) show the line-source solution in Equation (2-18) is accurate if time is

$$\frac{(3.975 \times 10^5)\phi\mu c_t r_w^2}{k} < t < \frac{948\phi\mu c_t r_e^2}{k}. \quad (2\text{-}19)$$

When the argument of the Ei function, $\frac{948\phi\mu c_t r^2}{kt}$, is less than 0.01, Equation (2-18) can be further simplified using an approximation for the Ei function. This approximation for $x < 0.01$ is

$$E_i(-x) \approx \ln(1.781x). \tag{2-20}$$

Therefore, substituting the above equation into Equation (2-18) gives pressure as

$$p = p_i + \frac{70.6\, qB\mu}{kh}\left[\ln\left(\frac{1688\,\phi\mu c_t r^2}{kt}\right)\right]. \tag{2-21}$$

Bottom-hole pressure is calculated by substituting $r = r_w$ into Equation (2-21), and is given by

$$p_{wf} = p_i + \frac{70.6\, qB\mu}{kh}\left[\ln\left(\frac{1688\,\phi\mu c_t r_w^2}{kt}\right)\right]. \tag{2-22}$$

Equation (2-22) is the transient flow solution for single phase radial flow. The transient flow equation for a reservoir containing gas can be obtained in a similar way and it is given by (Economides et al., 2013)

$$p_p(p_i) - p_p(p_{wf}) = 1638\frac{Tq}{kh}\left[\log\frac{kt}{\phi(\mu c_t)_i r_w^2} - 3.23\right], \tag{2-23}$$

where T is reservoir temperature in $°R$ and q is the gas flow rate in $(Mscf/d)$. $p_p(p)$ is the real gas pseudo-pressure function and is defined as

$$p_P(p) = 2\int_{p_0}^{p}\frac{p}{\mu z}\,dp\,, \tag{2-24}$$

where p_0 is arbitrary reference pressure.

The diffusivity equation for a reservoir with multi-phase flow is similar to the diffusivity equation for single phase flow (Martin, 1959). The only difference is

the use of total mobility, λ_t, and a total compressibility c_t. The diffusivity equation for radial flow of a multi-phase system is given by

$$\frac{\partial^2 p}{\partial r^2} + \frac{1}{r}\frac{\partial p}{\partial r} = \frac{\phi c_t}{\lambda_t}\frac{\partial p}{\partial t}. \tag{2-25}$$

The total mobility of a three phase system is defined as

$$\lambda_t = \lambda_o + \lambda_g + \lambda_w = \frac{k_o}{\mu_o} + \frac{k_g}{\mu_g} + \frac{k_w}{\mu_w}, \tag{2-26}$$

and the total compressibility is given by

$$c_t = S_o c_o + S_g c_g + S_w c_w + c_f. \tag{2-27}$$

The similarity between the single phase and multi-phase flow equations implies that the solution to diffusivity equation of a single phase flow also applies to the multi-phase flow.

I used a water-gas flow system in my numerical simulations. The transient flow equation for multi-phase flow of a gas-water system is

$$p_{wf} = p_i + \frac{70.6\, qB}{\lambda_t h}\left[\ln\left(\frac{1688\, \phi c_t r_w^2}{\lambda_t t}\right)\right], \tag{2-28}$$

where

$$\lambda_t = \lambda_g + \lambda_w = \frac{k_g}{\mu_g} + \frac{k_w}{\mu_w} \tag{2-29}$$

and

$$c_t = S_g c_g + S_w c_w + c_f. \tag{2-30}$$

The solution to the multi-phase flow diffusivity equation assumes that the saturation gradients in drainage area of the well are small.

2.3.2 Principle of Superposition in Time

The principle of superposition in time is used to solve the variable rate production problem. **Figure 2-1** shows the time variation of flow rate during a B/C test. In a baseline/calibration test, the well goes through a series of water injection and shut-in schedules. The constant flow rate varies in discrete injection stages. Peters (2012) used the principle of superposition to find the solution of reservoir pressure during variable injection rate. I used this technique to find pressure as function of time during B/C test.

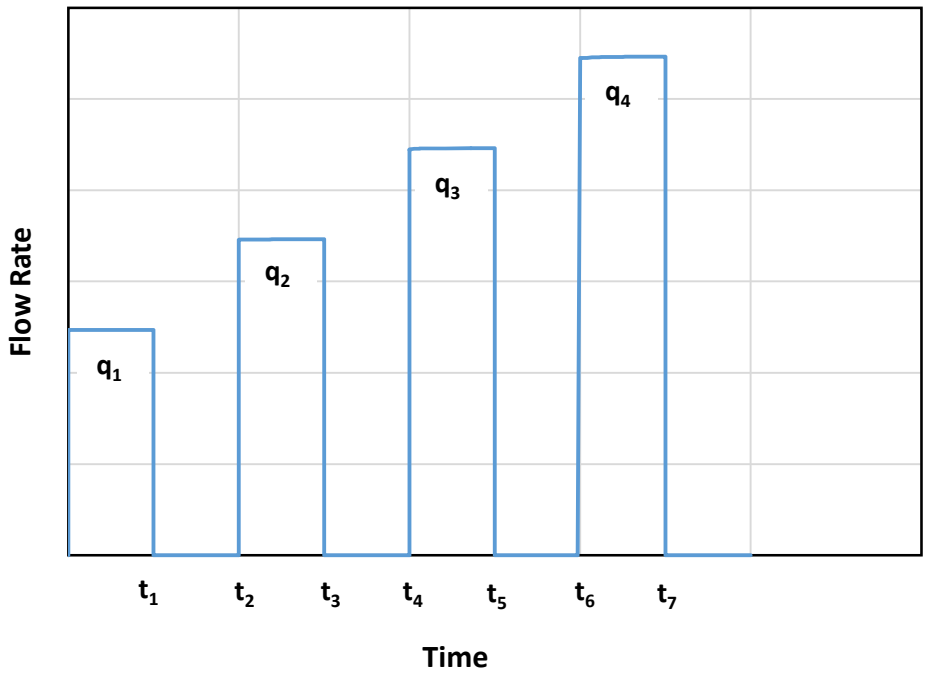

Figure 2-1: Constant flow rate injection during a baseline/calibration test.

According to the principle of superposition in time, when $t < t_7$, the dimensionless pressure solution is given by

$$p_D(r_D,t_D) = q_{1D}p_D(r_D,t_D) + (0-q_1)_D p_D[r_D,(t-t_1)_D] + (q_2-0)_D p_D[r_D,(t-t_2)_D] + (0-q_2)_D p_D[r_D,(t-t_3)_D] + (q_3-0)_D p_D[r_D,(t-t_4)_D] + (0-q_3)_D p_D[r_D,(t-t_5)_D] + (q_4-0)_D p_D[r_D,(t-t_6)_D] + (0-q_4)_D p_D[r_D,(t-t_7)_D], \quad (2\text{-}31)$$

where

$$p_D(r_D,t_D) = -\frac{1}{2}\,Ei\left(-\frac{r_D^2}{4t_D}\right) \text{ and} \quad (2\text{-}32)$$

$$p_D[r_D,(t-t_1)_D] = -\frac{1}{2}\,Ei\left(-\frac{r_D^2}{4(t-t_1)_D}\right). \quad (2\text{-}33)$$

The other dimensionless pressures are calculated from equations similar to Equation (2-33). Dimensionless flow rate is defined as

$$q_{1D} = \frac{q_1}{q_0}, \quad (2\text{-}34)$$

where q_0 is the reference flow rate which is usually assumed to be the flow rate in the first stage, i.e., $q_0 = q_1$ (Lee et al., 2003).

At the wellbore $r_D = 1$, hence, the dimensionless bottom-hole pressure is calculated by

$$p_{wD}(t_D) = q_{1D}p_D(t_D) + (-q_1)_D p_D[(t-t_1)_D] + (q_2)_D p_D[(t-t_2)_D] + (-q_2)_D p_D[(t-t_3)_D] + (q_3)_D p_D[r_D,(t-t_4)_D] + (-q_3)_D p_D[(t-t_5)_D] + (q_4)_D p_D[(t-t_6)_D] + (-q_4)_D p_D[(t-t_7)_D]. \quad (2\text{-}35)$$

By substituting the dimensionless parameters and using the approximation of Ei function, Equation (2-35) becomes

$$\frac{(p_i - p_{\mathrm{wf}})kh}{141.2q_1B_w\mu} = -\frac{1}{2}\left[\frac{q_1}{q_1}\ln\left(\frac{1688\,\phi\mu c_t r_w^2}{kt}\right) - \frac{q_1}{q_1}\ln\left(\frac{1688\,\phi\mu c_t r_w^2}{k(t-t_1)}\right)\right.$$

$$+\frac{q_2}{q_1}\ln\left(\frac{1688\,\phi\mu c_t r_w^2}{k(t-t_2)}\right) - \frac{q_2}{q_1}\ln\left(\frac{1688\,\phi\mu c_t r_w^2}{k(t-t_3)}\right)$$

$$+\frac{q_3}{q_1}\ln\left(\frac{1688\,\phi\mu c_t r_w^2}{k(t-t_4)}\right) - \frac{q_3}{q_1}\ln\left(\frac{1688\,\phi\mu c_t r_w^2}{k(t-t_5)}\right)$$

$$\left.+\frac{q_4}{q_1}\ln\left(\frac{1688\,\phi\mu c_t r_w^2}{k(t-t_6)}\right) - \frac{q_4}{q_1}\ln\left(\frac{1688\,\phi\mu c_t r_w^2}{k(t-t_7)}\right)\right]. \qquad (2\text{-}36)$$

Equation (2-36) applies to a reservoir with single phase liquid flow. The pressure solution for two phase flow is similar to single phase flow. The only difference is the use of total mobility and total compressibility. Therefore, for a reservoir containing gas and water, pressure response is

$$\frac{(p_i - p_{\mathrm{wf}})\lambda_t h}{141.2q_1B_w} = -\frac{1}{2}\left[\frac{q_1}{q_1}\ln\left(\frac{1688\,\phi c_t r_w^2}{\lambda_t t}\right) - \frac{q_1}{q_1}\ln\left(\frac{1688\,\phi c_t r_w^2}{\lambda_t(t-t_1)}\right)\right.$$

$$+\frac{q_2}{q_1}\ln\left(\frac{1688\,\phi c_t r_w^2}{\lambda_t(t-t_2)}\right) - \frac{q_2}{q_1}\ln\left(\frac{1688\,\phi c_t r_w^2}{\lambda_t(t-t_3)}\right)$$

$$+\frac{q_3}{q_1}\ln\left(\frac{1688\,\phi c_t r_w^2}{\lambda_t(t-t_4)}\right) - \frac{q_3}{q_1}\ln\left(\frac{1688\,\phi c_t r_w^2}{\lambda_t(t-t_5)}\right)$$

$$\left.+\frac{q_4}{q_1}\ln\left(\frac{1688\,\phi c_t r_w^2}{\lambda_t(t-t_6)}\right) - \frac{q_4}{q_1}\ln\left(\frac{1688\,\phi c_t r_w^2}{\lambda_t(t-t_7)}\right)\right], \qquad (2\text{-}37)$$

where

$$\lambda_t = \lambda_g + \lambda_w = \frac{k_g}{\mu_g} + \frac{k_w}{\mu_w} \qquad (2\text{-}38)$$

and

$$c_t = S_g c_g + S_w c_w + c_f. \qquad (2\text{-}39)$$

In order to calculate average reservoir pressure, I define t^* as the time at the onset of injection. Average reservoir pressure is expressed in Equation (2-40),

$$\bar{p} - p_{wf} = f(t^*) \text{ and} \tag{2-40}$$

$$\bar{p} = p_{wf} + f(t^*). \tag{2-41}$$

On the other hand, I showed that $p_i - p_{wf}$ is a function of time, i.e.,

$$p_i - p_{wf} = f(t) \text{ and} \tag{2-42}$$

$$p_{wf} = p_i - f(t). \tag{2-43}$$

By substituting Equation (2-43) in Equation (2-41), I obtain

$$\bar{p} = p_i - f(t) + f(t^*). \tag{2-44}$$

Average pressure, $\bar{p}$, defined by Equation (2-40) is expressed as

$$\bar{p} - p_{wf} = \frac{-70.6\, q_1 B_w}{\lambda_t h}\left[-\frac{q_4}{q_1}\ln\left(\frac{1688\,\phi c_t r_w^2}{\lambda_t(t-t^*)}\right)\right]. \tag{2-45}$$

Therefore, $\mathrm{f(t^*)}$ corresponding to Equation (2-40) is given by

$$\mathrm{f(t^*)} = \frac{-70.6\,\mathrm{q_1 B_w}}{\lambda_t \mathrm{h}}\left[-\frac{\mathrm{q_4}}{\mathrm{q_1}}\ln\left(\frac{1688\,\phi \mathrm{c_t r_w^2}}{\lambda_t(\mathrm{t}-\mathrm{t^*})}\right)\right]. \tag{2-46}$$

Similarly, I used Equation (2-37) to find $\mathrm{f(t)}$:

$$\begin{aligned} f(t) = \frac{-70.6\, B_w q_1}{\lambda_t h}\,[&\frac{q_1}{q_1}\ln\left(\frac{1688\,\phi c_t r_w^2}{\lambda_t t}\right) - \frac{q_1}{q_1}\ln\left(\frac{1688\,\phi c_t r_w^2}{\lambda_t(t-t_1)}\right) \\ &+\frac{q_2}{q_1}\ln\left(\frac{1688\,\phi c_t r_w^2}{\lambda_t(t-t_2)}\right) - \frac{q_2}{q_1}\ln\left(\frac{1688\,\phi c_t r_w^2}{\lambda_t(t-t_3)}\right) \\ &+\frac{q_3}{q_1}\ln\left(\frac{1688\,\phi c_t r_w^2}{\lambda_t(t-t_4)}\right) - \frac{q_3}{q_1}\ln\left(\frac{1688\,\phi c_t r_w^2}{\lambda_t(t-t_5)}\right) \\ &+\frac{q_4}{q_1}\ln\left(\frac{1688\,\phi c_t r_w^2}{\lambda_t(t-t_6)}\right) - \frac{q_4}{q_1}\ln\left(\frac{1688\,\phi c_t r_w^2}{\lambda_t(t-t_7)}\right)]. \end{aligned} \tag{2-47}$$

Substituting $f(t)$ and $f(t^*)$ into Equation (2-44), yields

$$\bar{p} = p_i + \frac{70.6\, B_w q_1}{\lambda_t h}\left[\frac{q_1}{q_1}\ln\left(\frac{1688\,\phi c_t r_w^2}{\lambda_t t}\right) - \frac{q_1}{q_1}\ln\left(\frac{1688\,\phi c_t r_w^2}{\lambda_t (t-t_1)}\right)\right.$$
$$+\frac{q_2}{q_1}\ln\left(\frac{1688\,\phi c_t r_w^2}{\lambda_t (t-t_2)}\right) - \frac{q_2}{q_1}\ln\left(\frac{1688\,\phi c_t r_w^2}{\lambda_t (t-t_3)}\right)$$
$$+\frac{q_3}{q_1}\ln\left(\frac{1688\,\phi c_t r_w^2}{\lambda_t (t-t_4)}\right) - \frac{q_3}{q_1}\ln\left(\frac{1688\,\phi c_t r_w^2}{\lambda_t (t-t_5)}\right) \qquad (2\text{-}48)$$
$$+\frac{q_4}{q_1}\ln\left(\frac{1688\,\phi c_t r_w^2}{\lambda_t (t-t_6)}\right) - \frac{q_4}{q_1}\ln\left(\frac{1688\,\phi c_t r_w^2}{\lambda_t (t-t_7)}\right)$$
$$\left.+\frac{q_4}{q_1}\ln\left(\frac{1688\,\phi c_t r_w^2}{\lambda_t (t-t^*)}\right)\right].$$

2.3.3 Piston-Like Displacement of Gas by Water

During a baseline/calibration test procedure, water is injected into the reservoir which creates a piston-like displacement profile within a distance from the wellbore. This distance is called the radius of invasion (r_e). The radius of invasion is a function of time and cumulative water injected. Assuming piston-like displacement of gas by water, radius of invasion can be calculated using a volumetric equation (Satter et al., 2008), namely,

$$Q = 5.615\,\phi A h\left(1 - S_{wi} - S_{gr}\right), \qquad (2\text{-}49)$$

where Q is total water injected in bbl, S_{wi} is initial water saturation (unitless), and S_{gr} is residual gas saturation (unitless). A is the area in ft^2, and is given by

$$A = \pi(r_e^2 - r_w^2). \qquad (2\text{-}50)$$

By substituting Equation (2-50) in Equation (2-49), I can found r_e as a function of cumulative injected water, porosity, thickness, wellbore radius, initial water saturation, and residual gas saturation, namely,

$$r_e = \sqrt{\frac{5.615\ Q}{\phi\pi h\left(1 - S_{wi} - S_{gr}\right)} + r_w^2}\ , \tag{2-51}$$

Because water is much more viscous than gas, it is plausible to assume a piston-like water displacement profile during water injection. In the radius of invasion, the pressure response is governed by a steady-state pressure gradient, that is,

$$\Delta p_{ww} = \frac{141.2\ q(t)B_w}{\lambda_w h}\ln(\frac{r_e}{r_w}), \tag{2-52}$$

where $q(t)$ is the injection rate in STB/d (Peters, 2012).

2.3.4 Superposition of Steady-State and Transient Pressures

Using results from previous sections, I superposed the pressure gradient across the piston-like profile of water and through water to outer reservoir boundary to obtain the pressure response at the wellbore during a B/C test. In other words, the pressure at the wellbore is a combination of the steady-state pressure gradient (Equation (2-52)) and the transient pressure response (Equation (2-37)), namely,

$$p_{wf} = \Delta p_{ww} + p_{trans}. \tag{2-53}$$

In the above equation

$$\begin{aligned} p_{trans} = p_i + \frac{141.2 q_1 B_w}{2\lambda_t h}[&\frac{q_1}{q_1}\ln\left(\frac{1688\ \phi c_t r_w^2}{\lambda_t t}\right) - \frac{q_1}{q_1}\ln\left(\frac{1688\ \phi c_t r_w^2}{\lambda_t (t - t_1)}\right) \\ &+ \frac{q_2}{q_1}\ln\left(\frac{1688\ \phi c_t r_w^2}{\lambda_t (t - t_2)}\right) - \frac{q_2}{q_1}\ln\left(\frac{1688\ \phi c_t r_w^2}{\lambda_t (t - t_3)}\right) \\ &+ \frac{q_3}{q_1}\ln\left(\frac{1688\ \phi c_t r_w^2}{\lambda_t (t - t_4)}\right) - \frac{q_3}{q_1}\ln\left(\frac{1688\ \phi c_t r_w^2}{\lambda_t (t - t_5)}\right) \\ &+ \frac{q_4}{q_1}\ln\left(\frac{1688\ \phi c_t r_w^2}{\lambda_t (t - t_6)}\right) - \frac{q_4}{q_1}\ln\left(\frac{1688\ \phi c_t r_w^2}{\lambda_t (t - t_7)}\right)], \end{aligned} \tag{2-54}$$

for $t > t_7$, and p_{ww} is calculated using Equation (2-52).

2.4 B/C Analysis - Pressure Calculation

In this work, I discuss only the mathematical formulations for the B/C test performed under injection with constant flow rate. Sandface flow rate and pressure pairs are recorded during a baseline/calibration test. The analysis of these data consists of a plot of $ln\left(\frac{r_e}{r_w}\right)$ versus $\Delta p/q$. $\Delta p/q$ is given by

$$\frac{\Delta p}{q} = \frac{p_{bh} - p_i}{q}, \tag{2-55}$$

and r_e is calculated using Equation (2-51). According to Equation (2-54), when $t < t_1$, p_{trans} is

$$p_{trans} = p_i + \frac{141.2 q_1 B_w}{2\lambda_t h}\left[\frac{q_1}{q_1}\ln\left(\frac{1688\,\phi c_t r_w^2}{\lambda_t t}\right)\right]. \tag{2-56}$$

If I assume $r_e^2 = \frac{kt}{1688\phi\mu c_t}$, then p_{trans} can be calculated as

$$p_{trans} = p_i - \frac{141.2 q_1 B_w}{2\lambda_t h}\left[\ln\left(\frac{r_e^2}{r_w^2}\right)\right] = p_i - \frac{141.2 q_1 B_w}{\lambda_t h}\ln\left(\frac{r_e}{r_w}\right). \tag{2-57}$$

Therefore p_{wf} is calculated using

$$\begin{aligned} p_{wf} &= p_{trans} + \Delta p_{ww} \\ &= p_i - \frac{141.2 q_1 B_w}{\lambda_t h}\ln\left(\frac{r_e}{r_w}\right) + \frac{141.2\, q_1 B_w}{\lambda_w h}\ln\left(\frac{r_e}{r_w}\right) \end{aligned} \tag{2-58}$$

$$= p_i + \frac{141.2 q_1 B_w}{h}\left[\frac{1}{\lambda_w} - \frac{1}{\lambda_t}\right]\ln\left(\frac{r_e}{r_w}\right).$$

By rearranging the above equation, I obtain

$$\frac{p_{bh} - p_i}{q_1} = \frac{141.2 B_w}{h}\left[\frac{1}{\lambda_w} - \frac{1}{\lambda_t}\right]\ln\left(\frac{r_e}{r_w}\right). \quad (2\text{-}59)$$

Similarly, for other time intervals, $\Delta p/q$ can be expressed similar to Equation (2-59). According to Equation (2-59), a plot of $\ln\left(\frac{r_e}{r_w}\right)$ versus $\Delta p/q$ should be linear for a correct assumption of initial reservoir pressure. In the B/C technique, a plot of the first injection stage generates a baseline trend and the plot for the second injection stage generates a calibration trend (see **Figure 2-2**). These trend lines align linearly if the assumed reservoir pressure is correct. If the assumed reservoir pressure is too high, then the two trend lines do not align and the calibration trend shifts to the right of baseline trend. On the other hand, if the assumed reservoir pressure is too low, then the calibration trend shifts to the left of baseline trend (Adams et al., 2013). Therefore, in an iterative manner, reservoir pressure can be estimated by calibrating the baseline.

Additional injection stages provide more baseline and calibration trends. For instance, the second injection stage can be a baseline trend where the third injection stage is the calibration trend, and this sequence continues. Each pair of baseline and calibration trends is aligned at a value which is an estimate of reservoir pressure. Each pair yields a separate estimated initial reservoir pressure; the collection of these pairs provides multiple values as reservoir

pressure. Each injection stage disturbs the formation, hence, the B/C technique find different initial pressure (Abdollah-Pour, 2011). Therefore, a correction method is designed to correct the baseline/calibration supercharging near the wellbore which is caused by injection.

Figure 2-2 demonstrates the trend alignment for a B/C test with three injection stages. This is the results of a numerical simulation where assumed reservoir pressure is 5250 psi. The B/C analysis shows the first pair of baseline/calibration trends are in alignment at $p_i = 5290\, psi$, and the second pair of baseline/calibration trends are aligned at $p_i = 5345\, psi$. Note that the estimated reservoir pressure increases from 5290 psi to 5320 psi from the first pair to the second pair. This effect is called B/C supercharging (Adams et al., 2013). To correct the B/C supercharging, matching pressure points are plotted versus the corresponding cumulative injection water. A linear trend line passes through these points and extrapolated back to the zero cumulative injection as shown in **Figure 2-3**. The final estimate of reservoir pressure is the pressure at the zero cumulative water injection where reservoir has not been disturbed yet.

2.5 B/C Analysis- Permeability Calculation

Using baseline/calibration analysis, I develop a method to estimate effective permeability to water phase in the reservoir. According to Equation (2-59), a plot of $\ln(\frac{r_e}{r_w})$ versus $\frac{\Delta p}{q}$ should be linear with a constant slope. This constant slope is given by

$$m = \frac{h}{141.2B_w}\left[\frac{1}{\lambda_w} - \frac{1}{\lambda_t}\right]^{-1}. \quad (2\text{-}60)$$

Since $\lambda_t \gg \lambda_w$, the term $1/\lambda_t$ can be neglected. Thus slope m is approximated as

$$m = \frac{k_w h}{141.2\mu B_w}. \quad (2\text{-}61)$$

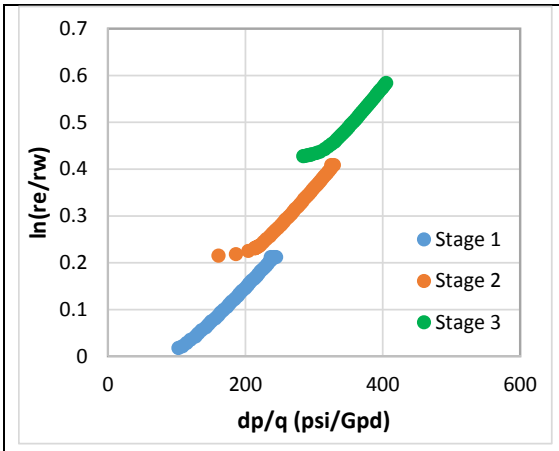

(a) $p_i = 5100\,psi$, calibration trends are shifted to left meaning the assumed p_i is too low.

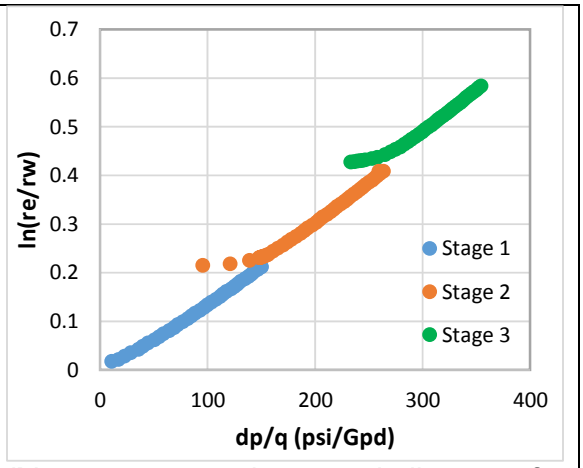

(b) $p_i = 5290\,psi$, best trend alignment for stages 1 and 2.

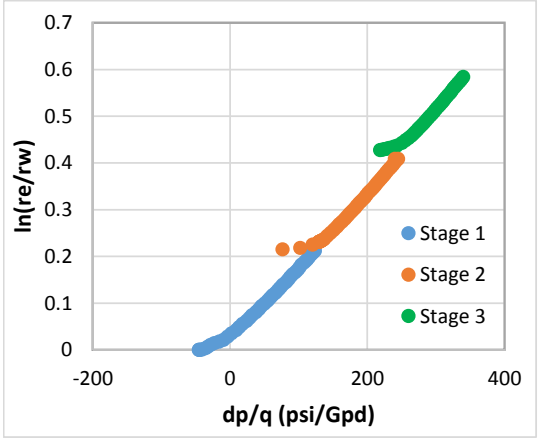

(c) $p_i = 5345\,psi$, best trend alignment for stages 2 and 3.

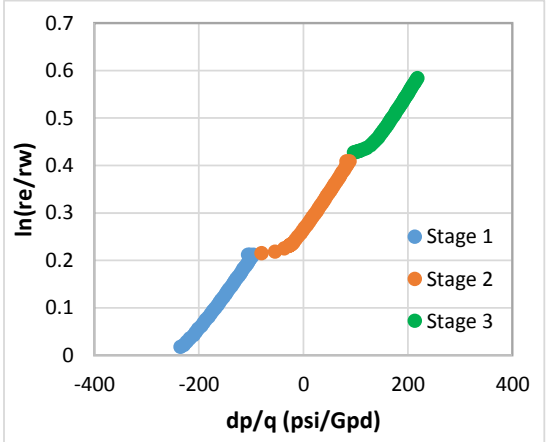

(d) $p_i = 5800\,psi$, calibration trends are shifted to right meaning the assumed p_i is too high.

Figure 2-2: Baseline/calibration trend alignment.

I used the slope of the alignment of the last pair to find the effective permeability of water. Using known values of fluid viscosity, thickness, and water formation volume factor, effective permeability of water is calculated as

$$k_{wef} = \frac{141.2\mu B_w m}{h}. \tag{2-62}$$

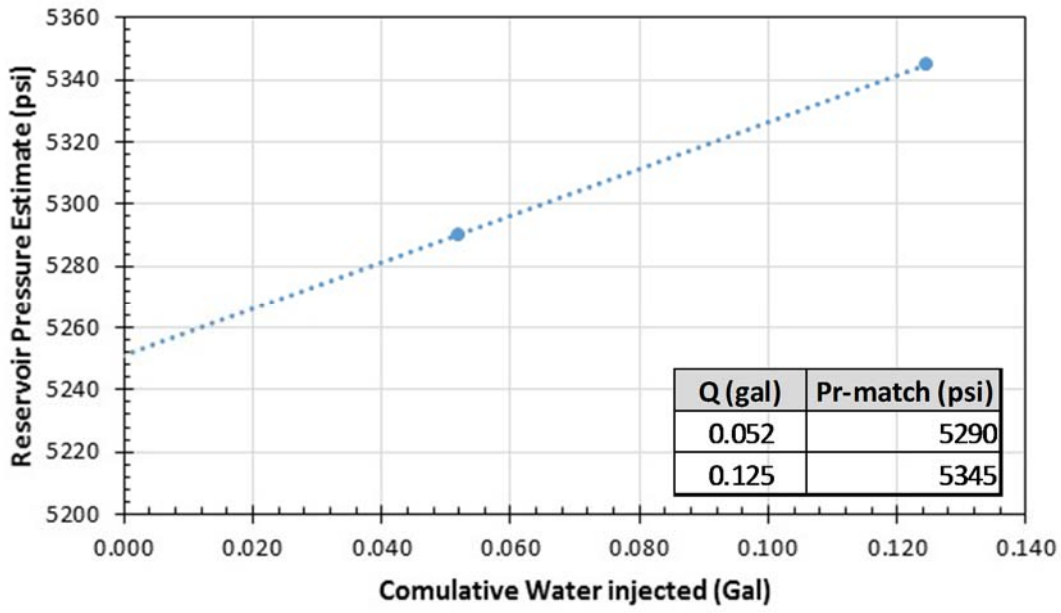

Figure 2-3: Baseline/Calibration supercharging correction. The alignment pressures are plotted versus the corresponding cumulative injected water. A linear trend line passes through these points and extrapolated back to the zero cumulative injection. The final estimate of reservoir pressure is 5250 psi.

Chapter 3

Numerical Model Simulation

3.1 Introduction

In this chapter, I present several baseline/calibration test models constructed using a numerical simulation software to validate the results from this technique. I compared the results of baseline/calibration technique from simulator with those obtained from mathematical formulations I developed. I performed assessment of the validity of this method in formations with different permeabilities and defined the applicability range for baseline/calibration method.

I used a commercial reservoir simulator from Computer Modeling Group Ltd. (CMG). The variations of composition, phase behavior, and temperature are negligible in these tests. Hence, a conventional black oil simulator, CMG-IMEX was used to accurately model the case studies.

3.2 Reservoir description

In this study, a one dimensional (1D) radial reservoir model with a radius of 300 feet was constructed with 300x1x1 grids. A wellbore with 0.341 feet radius is located in the middle of the reservoir. Grid blocks are designed logarithmically to have smaller grids toward the wellbore and larger grids farther from the wellbore. **Figure 3-1** and **Figure 3-2** show two-dimensional (2D) top and side views of a numerical reservoir model in *i-j* and *i-k* directions, respectively. A

three dimensional (3D) grid top view of numerical simulation model is presented in **Figure 3-3**.

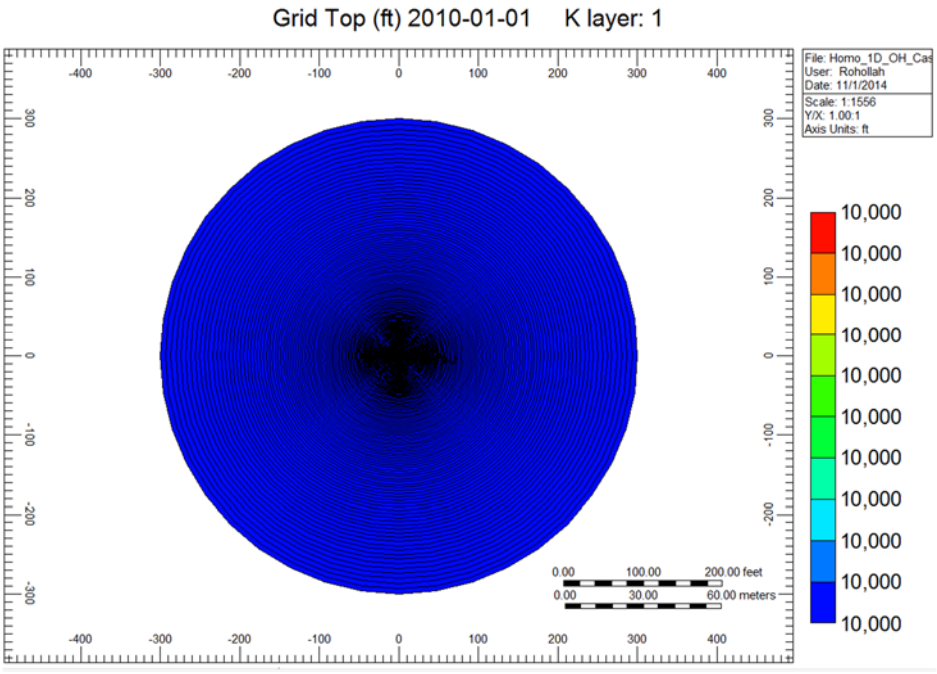

Figure 3-1: 2D grid top view of numerical reservoir model in I and J directions.

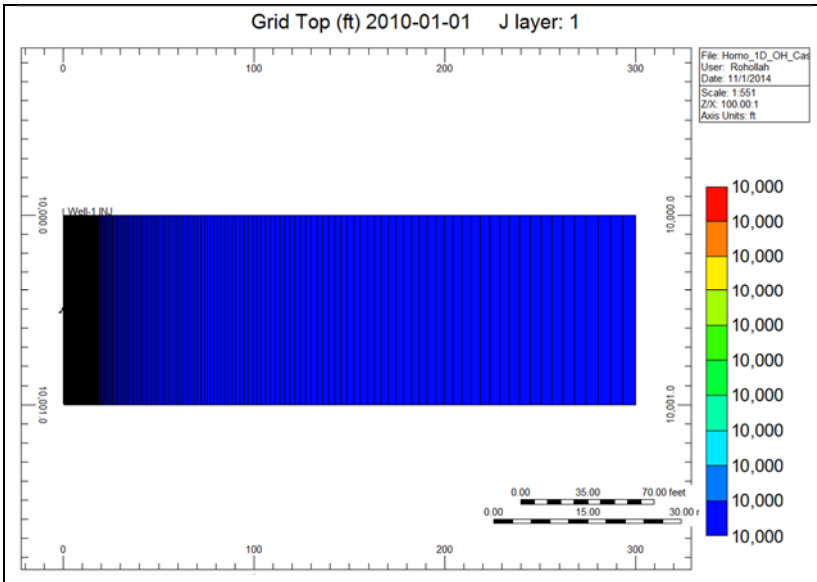

Figure 3-2: 2D grid top view of numerical reservoir model in I and K directions.

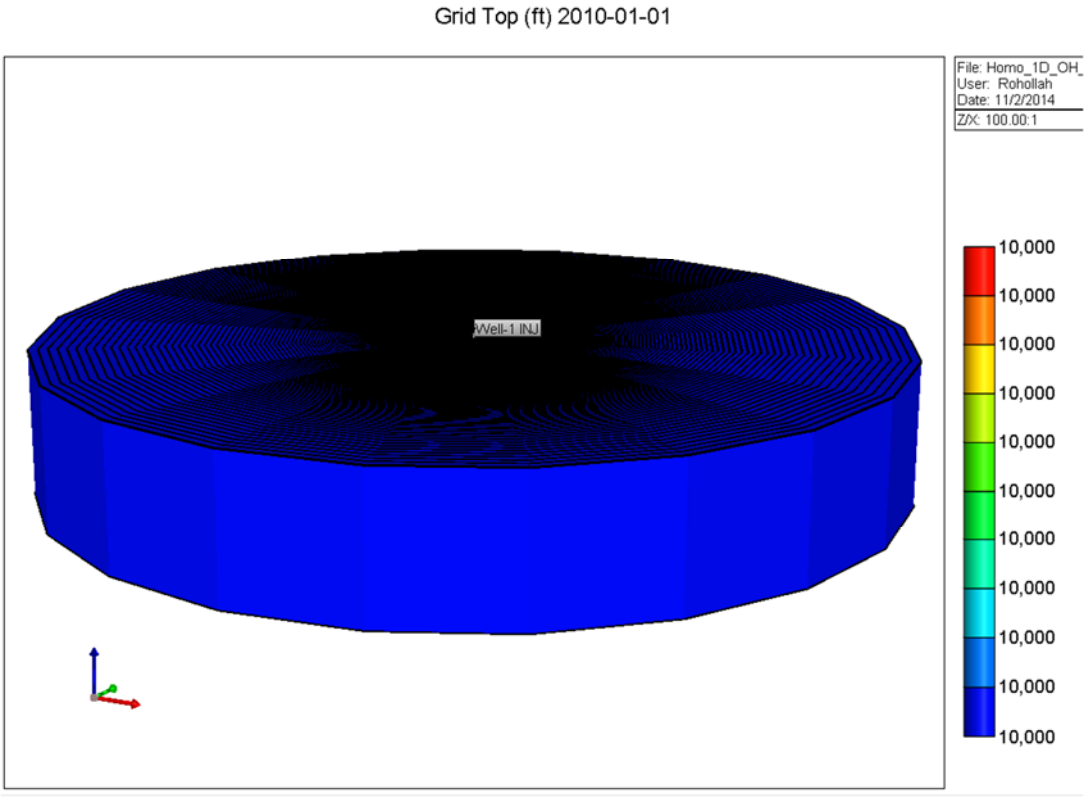

Figure 3-3: Three dimensional grid top view of numerical reservoir model.

3.2.1 Petrophysical Properties

The reservoir simulation model is assumed to have a porosity of 8 percent and initial water saturation of 20 percent. Previous experimental studies have shown that residual gas saturation under water drive can be extremely high, between 15 to 50 percent of pore volume (Geffen et al., 1952). A value of 35% of pore volume is often used in field practices when specific information about residual gas saturation is not available (Agarwal et al., 1965). Recently, Merletti et al. (2013) performed petrophysical evaluations of Wamsutter tight gas sand formations and found a range of 20 to 45 percent for residual gas saturation. In

this study, I chose value of 35 percent for residual gas saturation in all reservoir simulation models.

In this study, rock compressibility is assumed to be $2 \times 10^{-6}\ 1/psi$ at reference pressure of $5250\ psi$. For simplicity, the reservoir model thickness is assumed to be 1 ft. I set up three different numerical case studies, with formation permeability values of 0.001, 0.01, and 0.1 mD. I assess the validity of B/C technique on all case studies. In all of these reservoir models, k_v/k_H is assumed to be 0.1.

3.2.2 Fluid Properties

The numerical reservoir models with which the baseline/calibration technique was tested consisted of two phases; water and gas. **Table 3-1** describes properties of the water phase.

Table 3-1: Assumed properties of the water component

Parameter	Unit	Value
Water compressibility	1/psi	3.159 x 10^{-6}
Viscosity	cp	0.472
Density	lb/ft	61.638

Figure 3-4 shows assumed viscosity and formation volume factor for the gas phase in this study. Gas compressibility factor is a function of pressure and is shown in **Figure 3-5**.

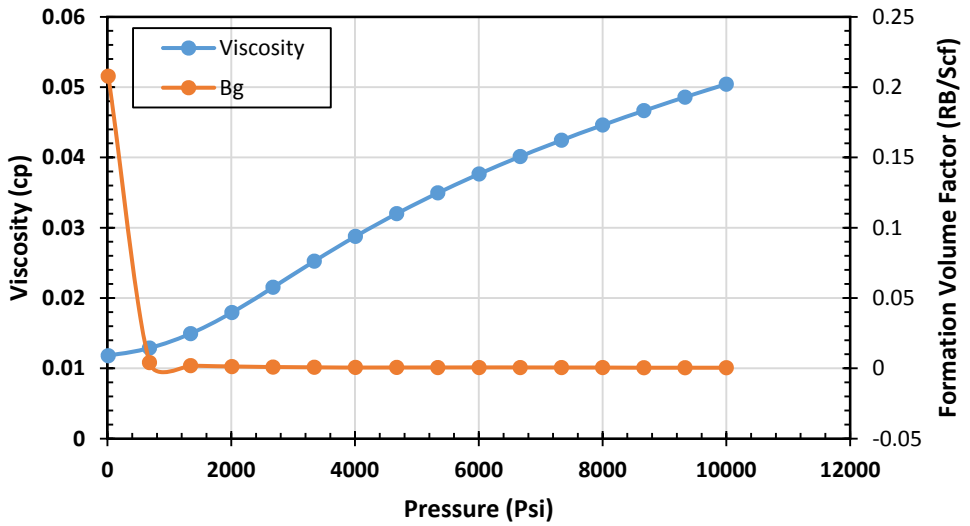

Figure 3-4: Gas formation volume factor and viscosity are functions of pressure in all reservoir simulation models.

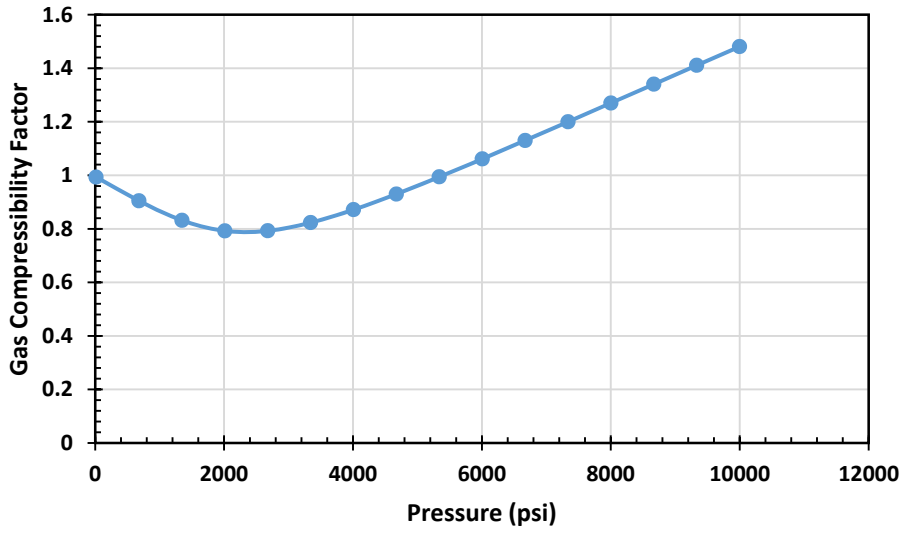

Figure 3-5: Assumed gas compressibility factor is a function of pressure in all reservoir simulation models.

3.2.3 Rock-Fluid Properties

I assume the formation rock is water wet and initial water saturation is 20 percent whereas residual gas saturation is 35 percent. **Figure 3-6** shows the assumed relative permeability curves for the reservoir rock model.

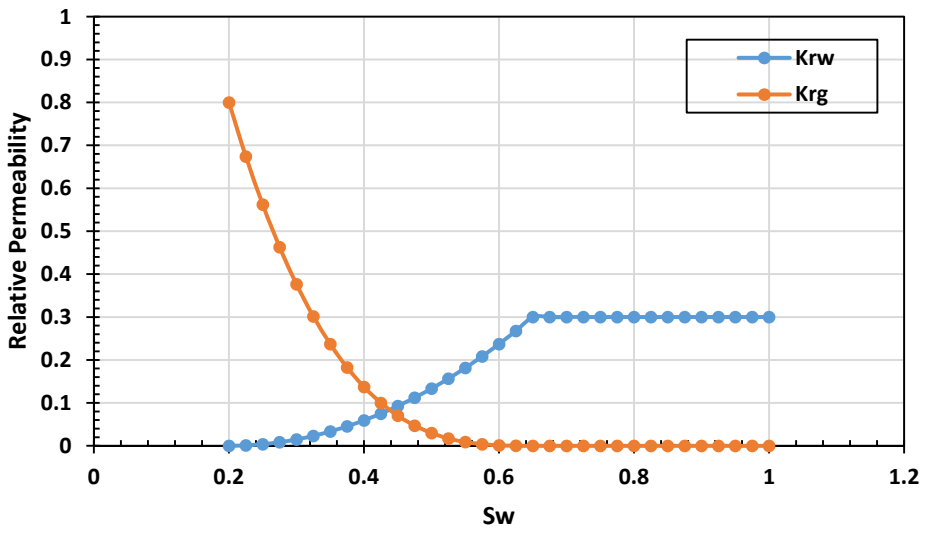

Figure 3-6: Relative permeability curves for the reservoir rock studied in this thesis. Variables k_{rg} and k_{rw} are relative permeability of gas and water, respectively.

3.2.4 Initial Conditions

Initial conditions for numerical reservoir model are described in **Table 3-2**. I assumed the depth of water-gas contact is 10,100 ft and at the reservoir depth, water is at the irreducible level.

3.3 Description of Validation Case Studies

For validation purposes and finding the range of formation permeability where baseline/calibration method is applicable, I created three different

reservoir simulation models, with permeabilities of 0.001, 0.01, 0.1 mD. In a recent study, Almond reservoir sands exhibited porosities in the range of 6 to 16 percent and absolute permeabilities ranging from 0.003 to 3 mD (Merletti et al., 2013). Merletti et al. (2013) showed that a single porosity value can exhibit permeabilities varying by 3 orders of magnitude (i.e. a rock with porosity value of 10 percent, have permeability ranges between 0.001mD to 1mD). I chose the same porosity of 8 percent for all of reservoir simulation rock types with different permeabilities.

Table 3-2: Initial conditions assumed for numerical reservoir model.

Parameter	Unit	Value
Reservoir Temperature	°F	150
Initial Reservoir Pressure	psi	5250
Reservoir Top Depth	ft	10000

I used a constant rate injection method to simulate the B/C test. For example for a reservoir with the permeability of 0.01 md, I modeled 4 different injection stages with constant rates of 0.05, 0.07, 0.09, and 0.11 bbl/day with 4 shut-in times between each set of two injection stages. Each injection stage and shut-in time lasted 36 minutes. **Figure 3-7** represents time variation of injection rate for B/C test when performed for a formation with permeability equal to 0.01 md.

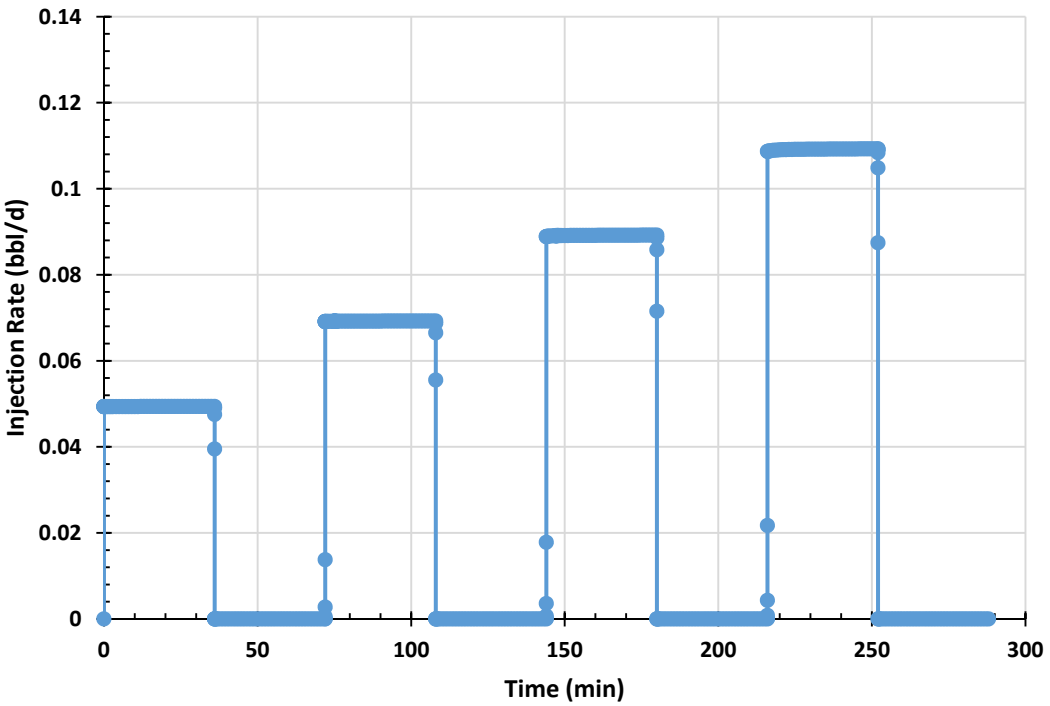

Figure 3-7: Time variation of injection rate for B/C test when performed for a formation with permeability equal to 0.01 mD.

Chapter 4

Results

4.1 Introduction

In this chapter, I present the validation of the mathematical formulations which were described in **Section 2.3**. For this purpose, I compared results obtained using mathematical formulations with those obtained from reservoir simulation models.

Initially, I studied the mathematical formulation corresponding to a reservoir containing single-phase water. Afterwards, I tested the mathematical formulations for a reservoir with two phases of water and gas. I present the results of the baseline/calibration test and analysis for different numerical simulation models.

4.2 Mathematical Solution for a Single-Phase Water

In simulation of a reservoir containing single phase water, I used the initial conditions summarized in **Table 3-2**. I assumed reservoir permeability is 0.01mD and the depth of water-gas contact is 9000 ft. Therefore, there is only a single phase water at the depth of assumed reservoir, 10,000 ft. In a B/C test procedure, the fluid injected was water; therefore, a single phase fluid flowed in this test case.

In this simulation, I assumed water injection in 4 stages. **Figure 4-1** shows the injection schedule.

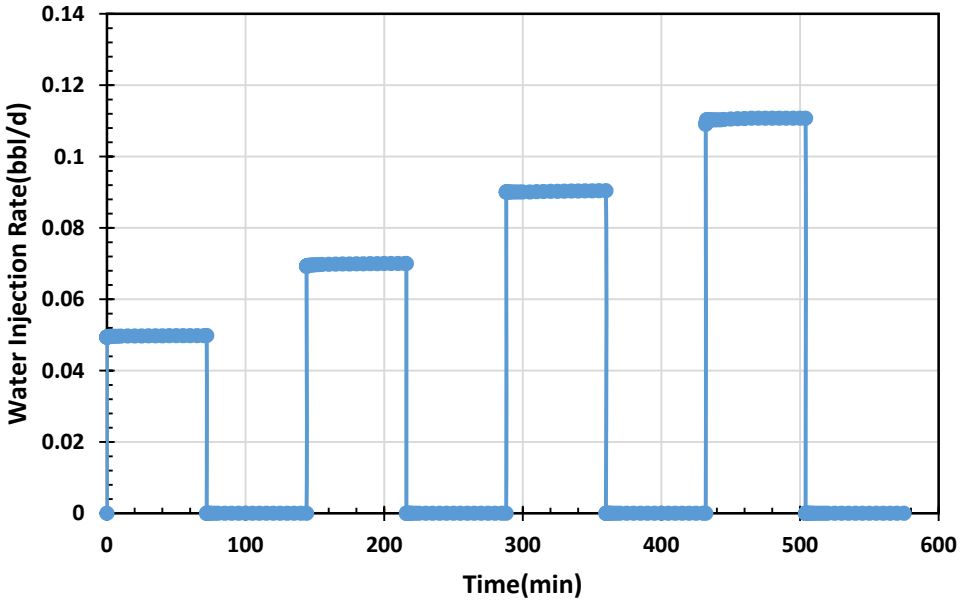

Figure 4-1: Schedule of constant injection rates in different stages for a numerical simulation model with single phase water.

The bottom-hole pressure is calculated using Equation (2-36). **Figure 4-2** compares the bottom-hole pressure obtained from simulator (solid black line) with those calculated using bottom-hole pressure of Equation (2-36), (dashed red line). Equation (2-36) was described as

$$\frac{(p_i - p_{\mathrm{wf}})kh}{141.2q_1B\mu} = -\frac{1}{2}\left[\frac{q_1}{q_1}\ln\left(\frac{1688\,\phi\mu c_t r_w^2}{kt}\right) - \frac{q_1}{q_1}\ln\left(\frac{1688\,\phi\mu c_t r_w^2}{k(t-t_1)}\right)\right.$$
$$+\frac{q_2}{q_1}\ln\left(\frac{1688\,\phi\mu c_t r_w^2}{k(t-t_2)}\right) - \frac{q_2}{q_1}\ln\left(\frac{1688\,\phi\mu c_t r_w^2}{k(t-t_3)}\right)$$
$$+\frac{q_3}{q_1}\ln\left(\frac{1688\,\phi\mu c_t r_w^2}{k(t-t_4)}\right) - \frac{q_3}{q_1}\ln\left(\frac{1688\,\phi\mu c_t r_w^2}{k(t-t_5)}\right)$$
$$\left.+\frac{q_4}{q_1}\ln\left(\frac{1688\,\phi\mu c_t r_w^2}{k(t-t_6)}\right) - \frac{q_4}{q_1}\ln\left(\frac{1688\,\phi\mu c_t r_w^2}{k(t-t_7)}\right)\right]. \qquad (2\text{-}36)$$

In **Figure 4-2**, calculated bottom-hole pressures do not exactly match bottom-hole pressures obtained from simulator for a very short time ($\Delta t < 10^{-6}$ day) at the onset of each injection stage. This is due to the fact that t_D is very small at the beginning of each stage, and the approximation of the Ei function is not accurate (see section **Solution to Diffusivity Equation**). If I use the Ei function instead of natural logarithm approximation in Equation (2-36), the calculated p_{wf} is identical to bottom-hole pressure results from simulator. **Figure 4-3** compares calculated p_{wf} using the Ei function to p_{wf} obtained from the simulator CMG-IMEX.

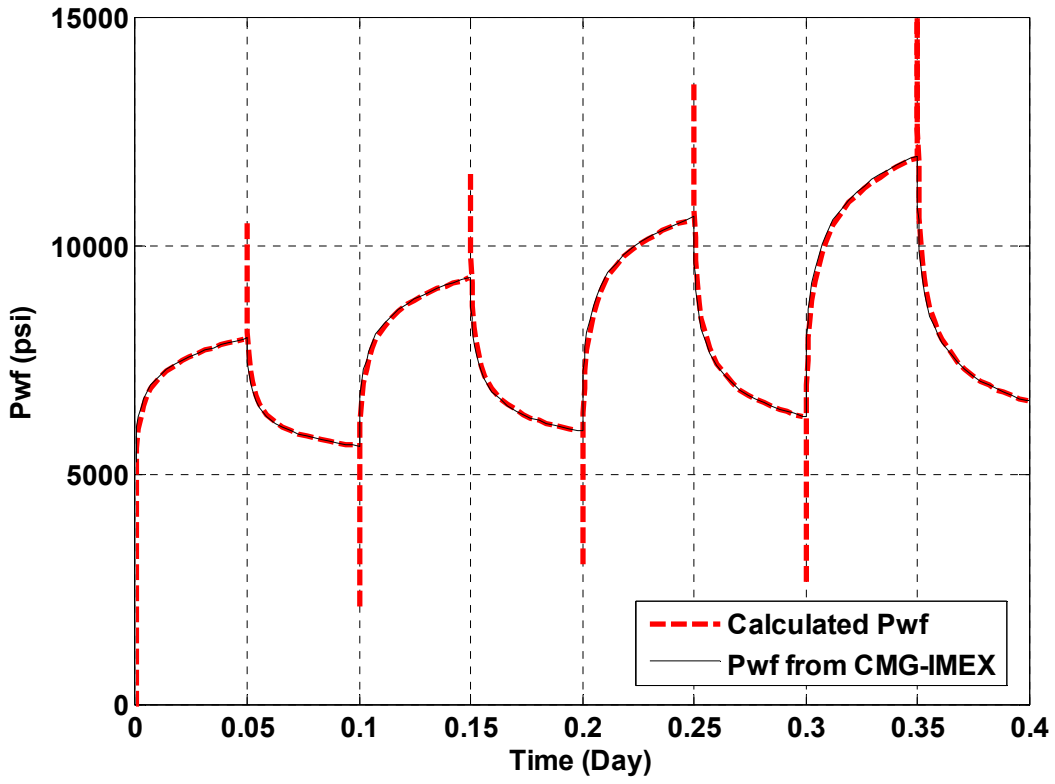

Figure 4-2: Comparison of calculated bottom-hole pressure with that obtained using **CMG-IMEX** for a simulation case study of single-phase water flow.

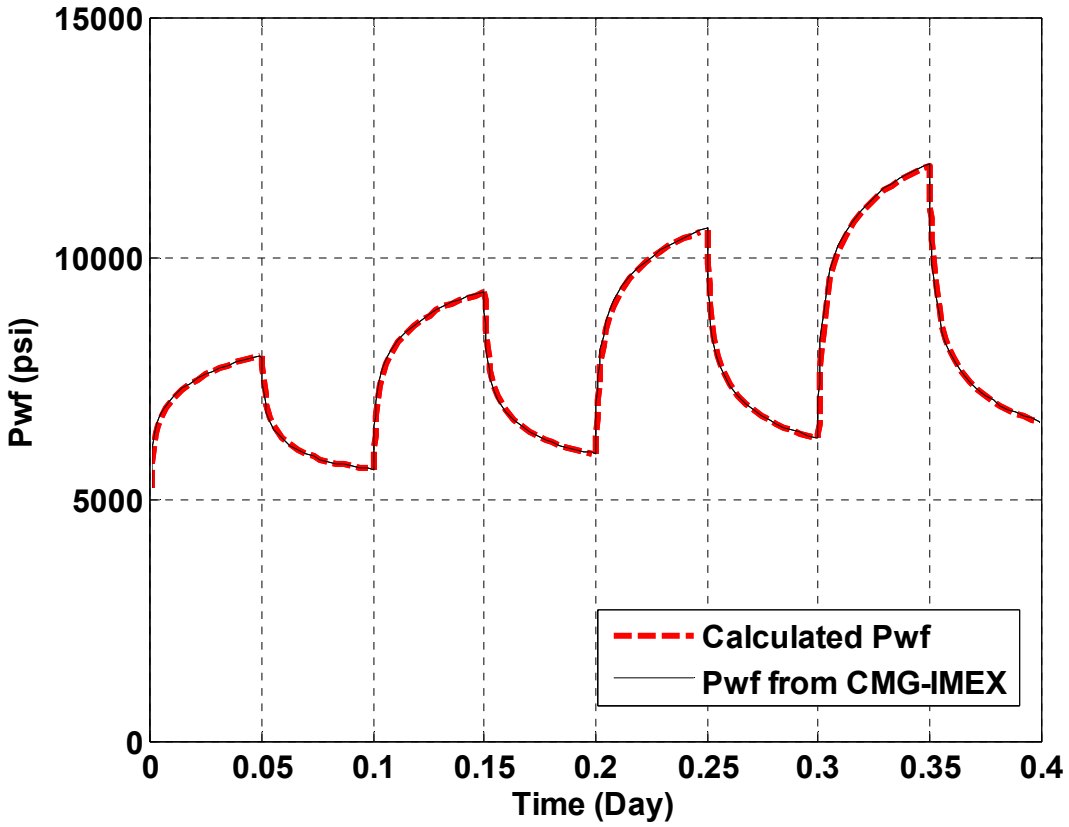

Figure 4-3: Comparison of bottom-hole pressure calculated with the Ei function and that obtained from CMG-IMEX for a simulation case study of single-phase water flow. In contrast to **Figure 4-2**, in this figure, E_i function is used instead of the logarithmic approximation to calculate bottom-hole pressure.

4.3 Mathematical Solution for Two-Phase Flow Gas and Water

For the simulation of a reservoir containing two phases, gas and water, I assumed the initial condition described in **Table 3-2**. I assumed formation permeability is 0.01 mD, reservoir depth is 10,000 ft, and the depth of water-gas contact is 10,100 ft. Therefore, at the reservoir depth, water saturation is at the irreducible level (20 percent in these simulations). I assumed petrophysical, fluid, and rock-fluid properties as described in **Chapter 3**.

I assumed injection of water in 4 discrete stages similar to that described in **Figure 3-7**. Each injection and shut-in stage lasted 36 minutes. The bottom-hole pressure for a two-phase flow is governed by Equation (2-53) as

$$p_{wf} = \Delta p_{ww} + p_{trans}, \tag{2-53}$$

where

$$p_{trans} = p_i + \frac{141.2 q_1 B}{2\lambda_t h}\left[\frac{q_1}{q_1}\ln\left(\frac{1688\,\phi c_t r_w^2}{\lambda_t t}\right) - \frac{q_1}{q_1}\ln\left(\frac{1688\,\phi c_t r_w^2}{\lambda_t (t-t_1)}\right)\right.$$

$$\ldots + \frac{q_2}{q_1}\ln\left(\frac{1688\,\phi c_t r_w^2}{\lambda_t (t-t_2)}\right) - \frac{q_2}{q_1}\ln\left(\frac{1688\,\phi c_t r_w^2}{\lambda_t (t-t_3)}\right)$$

$$\ldots + \frac{q_3}{q_1}\ln\left(\frac{1688\,\phi c_t r_w^2}{\lambda_t (t-t_4)}\right) - \frac{q_3}{q_1}\ln\left(\frac{1688\,\phi c_t r_w^2}{\lambda_t (t-t_5)}\right)$$

$$\left.\ldots + \frac{q_4}{q_1}\ln\left(\frac{1688\,\phi c_t r_w^2}{\lambda_t (t-t_6)}\right) - \frac{q_4}{q_1}\ln\left(\frac{1688\,\phi c_t r_w^2}{\lambda_t (t-t_7)}\right)\right] \tag{2-54}$$

and

$$\Delta p_{ww} = \frac{141.2\, q(t) B_w}{\lambda_w h}\ln\left(\frac{r_e}{r_w}\right). \tag{2-52}$$

Figure 4-4 compares the calculated bottom-hole pressures using Equation (2-53) with that obtained with numerical simulation. It is observed that bottom-hole pressure calculated using Equation (2-53) has a very good agreement with that obtained from numerical simulator.

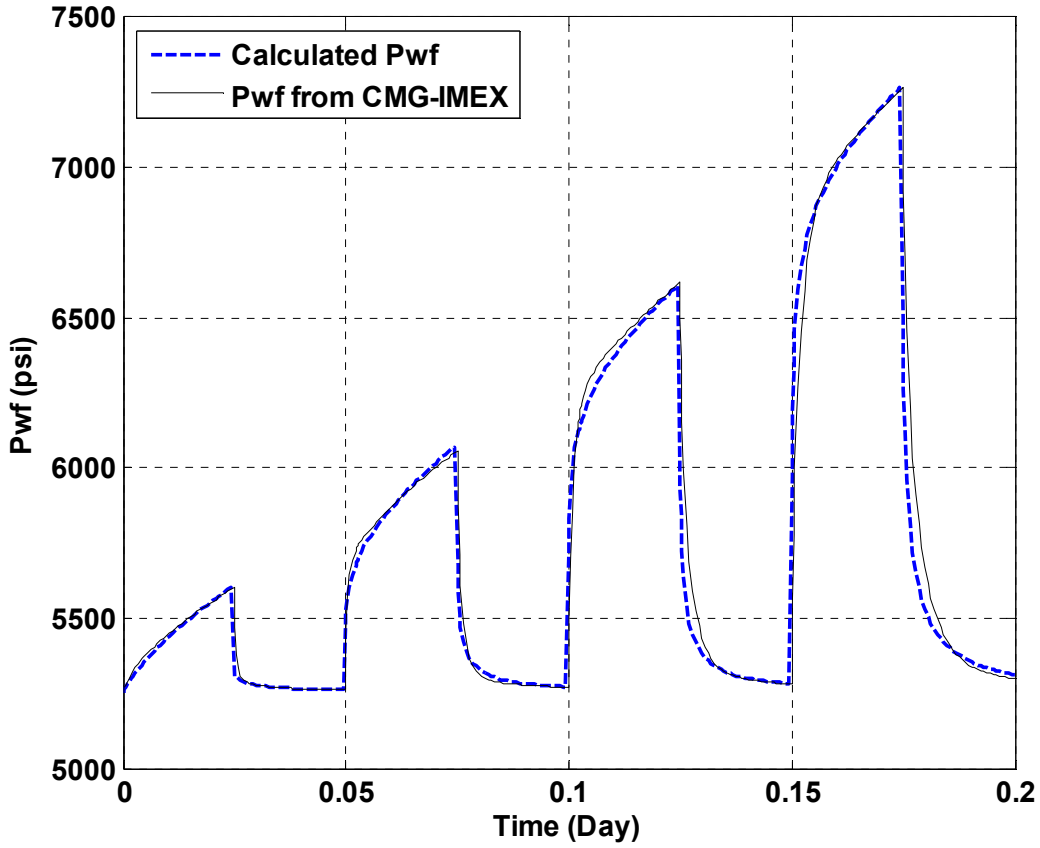

Figure 4-4: Comparison of calculated bottom-hole pressure with that obtained using simulator CMG-IMEX in a case study with two phases of gas and water. Formation permeability is assumed to be 0.01 mD.

4.4 Baseline/Calibration Case Studies

In this section, I present the validation of the baseline/calibration method using numerical case studies for formations with permeability values of 0.001, 0.01, and 0.1 mD. In all these simulations, both gas and water phases were flowing. Reservoir and fluid properties are those described in **Chapter 3**.

4.4.1 Formation with 0.01 mD Permeability

For the simulation of this case study of B/C test, I considered injection of water in 4 different stages as shown in **Figure 3-7**. **Figure 4-5** exhibits bottom-hole pressure and cumulative water injected during testing time from the simulator.

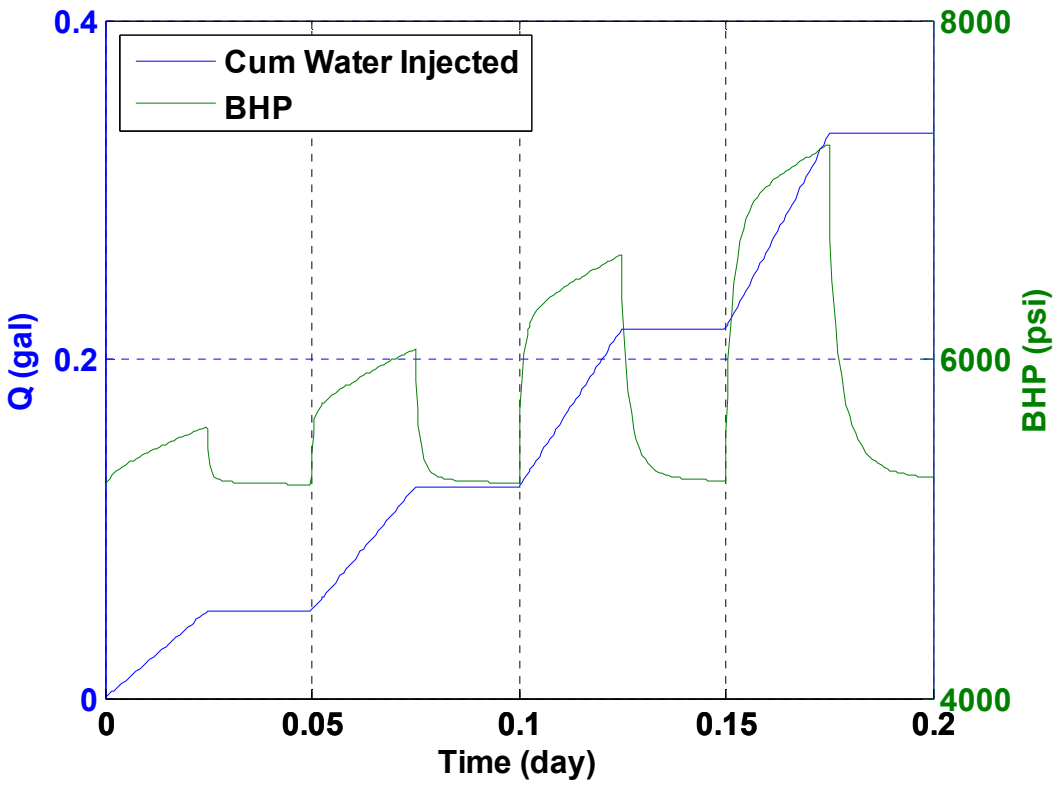

Figure 4-5: Numerical simulation output for a case study with two phases of gas and water. Formation permeability is assumed to be 0.01mD. This figure shows cumulative injected water and bottom-hole pressure (BHP) versus time.

Baseline/calibration analysis consists of a graph of $ln\left(\frac{r_e}{r_w}\right)$ versus $\frac{p_i - p_{wf}}{q}$. Initial pressure, p_i, is estimated through an iterative method by aligning each pair of baseline and calibration trends. **Figure 4-6** presents the

best alignment for first, second, and third pairs of baseline and calibration trends. Each injection stage disturbed the formation, hence, the B/C technique finds different pressures. **Table 4-1** shows that each pair of baseline and calibration trends is aligned at a different pressure. This is called the B/C supercharging effect and it needs to be corrected. Therefore, a correction method is designed to correct the baseline/calibration supercharging near the wellbore caused by injection.

Table 4-1 summarizes reservoir pressure from calibrated baseline method and their corresponding cumulative injected water. Moreover, the average slope of baseline and calibration trends for each pair (used to calculate permeability) are listed in **Table 4-1**.

Table 4-1: Summary of cumulative injected water, reservoir pressure match, and average slope for each pair of baseline/calibration trends. In this simulation, formation permeability is assumed to be 0.01 mD.

Pair	Q (gal)	P_r-match (psi)	Slope (Gpd/psi)
1	0.052	5258	0.0015
2	0.125	5274	0.0016
3	0.218	5284.2	0.0015

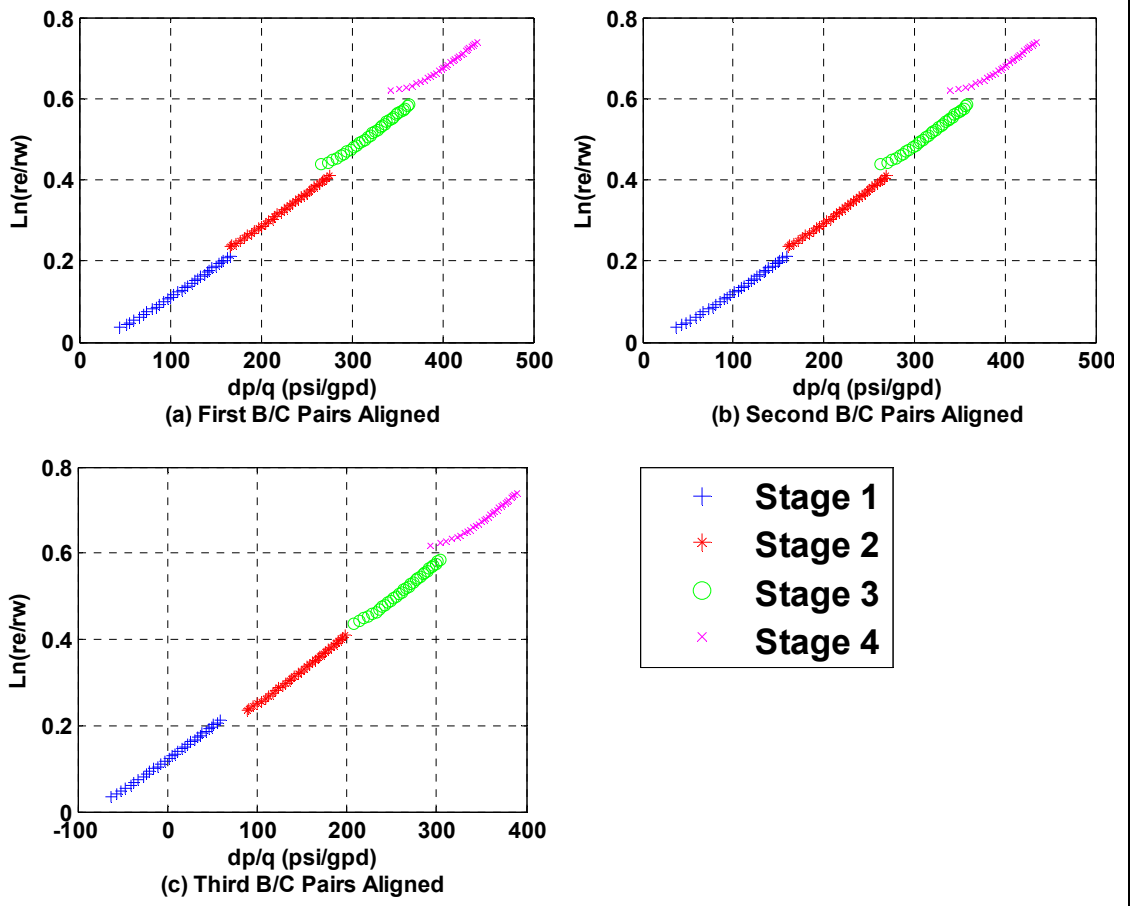

Figure 4-6: Baseline/calibration alignment for a numerical simulation model with permeability equal to 0.01 mD. (a) First B/C pair is aligned at 5258 psi, (b) second B/C pair is aligned at 5274 psi, and (c) third B/C pair is aligned at 5282.2 psi.

The baseline/calibration supercharging was corrected in the following way: (i) calibrated baseline reservoir pressures were plotted versus their cumulative injected water; (ii) a linear trend line was drawn through matching pressure points, and extrapolated to zero cumulative water injection; (iii) final estimated reservoir pressure is the pressure at zero cumulative injected water where reservoir was at initial condition. **Figure 4-7** shows B/C pressure and correction

of supercharging effect. Final estimate of reservoir pressure is 5251.7 psi with 0.032% error. The error was calculated by

$$error\% = \frac{p_{i,calculated} - p_{i,known}}{p_{i,known}} \times 100. \quad (4\text{-}1)$$

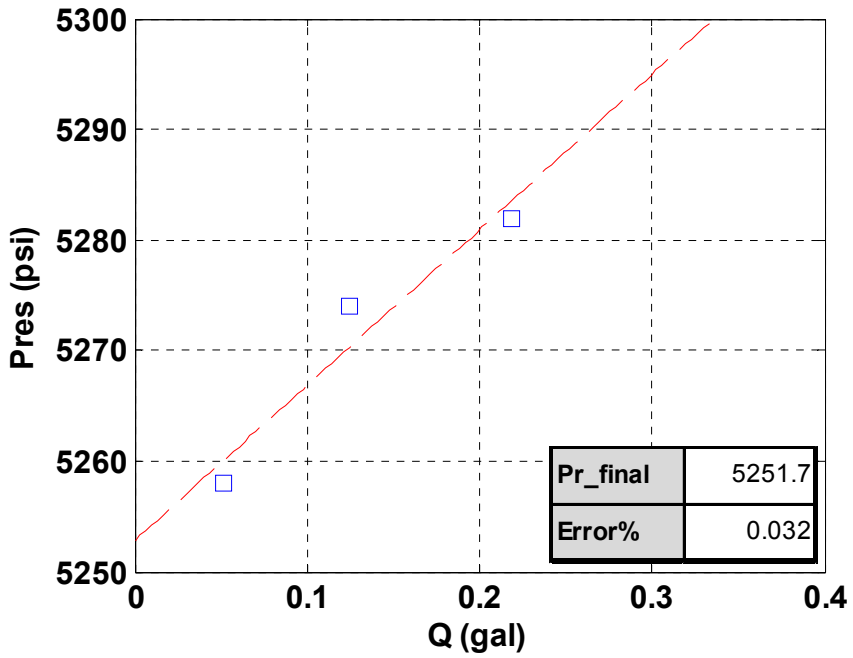

Figure 4-7: Baseline/calibration supercharging correction for a case study with permeability equal to 0.01 mD. The linear trend line passes through pressure match points and extrapolated to zero cumulative water injected. R^2 for the linear trend line is 0.96. The final estimate of initial reservoir pressure is 5251.7 psi.

In **Figure 4-8**, I compared the alignment matching pressure with average pressure within the invaded area. It turns out that alignment pressures are approximately the same as average pressures at the end of each shut-in time. **Figure 4-8** displays calculated average pressures versus cumulative injected water. Pressures at alignments are shown in blue point. **Figure 4-9** shows the

agreement between average pressure along the radius of invasion and alignment B/C pressures as a function of time.

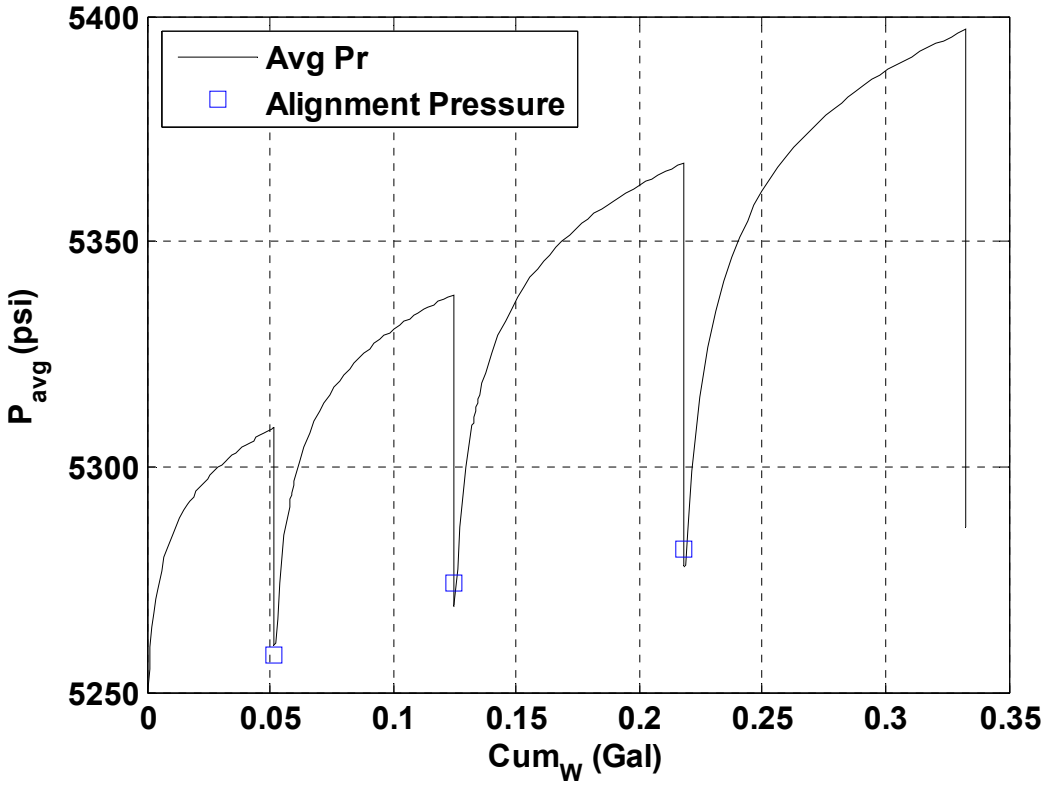

Figure 4-8: Average pressure of invaded area versus cumulative injection water. At onset of injection period between each pair, average pressures agree well with alignment B/C pressures.

Next, using Equation (2-62), I calculated effective water permeability equal to 0.0024 mD. The maximum value of effective water permeability for this simulation model was

$$k_{ew} = k_{abs} \times k_{rw} = 0.01 \times 0.3 = 0.003\, mD, \tag{4-2}$$

when $S_w = 1 - S_{rg}$.

During the simulated B/C test, as shown in **Figure 4-10**, water saturation does not reach to the maximum level, $1 - S_{rg}$. Therefore, the calculated k_{ew} of 0.0024 mD is less than 0.003 and represents the average effective water permeability in the radius of invasion. Using the rock-fluid properties, described in **Figure 3-6**, I estimated gas effective permeability as $k_{eg} = \frac{0.8}{0.3} * 0.0024 = 0.0064\, mD$.

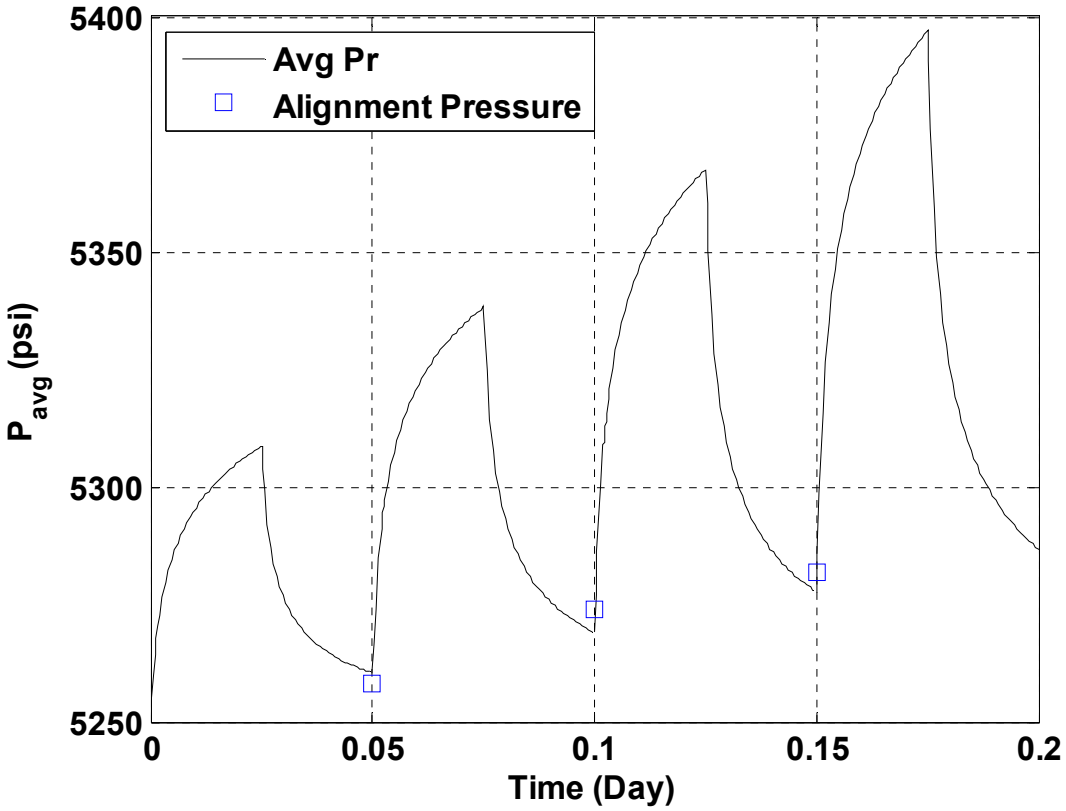

Figure 4-9: Average pressures of invaded zone versus time. Pressure alignment points are approximately the same as average pressures at the end of each shut-in time.

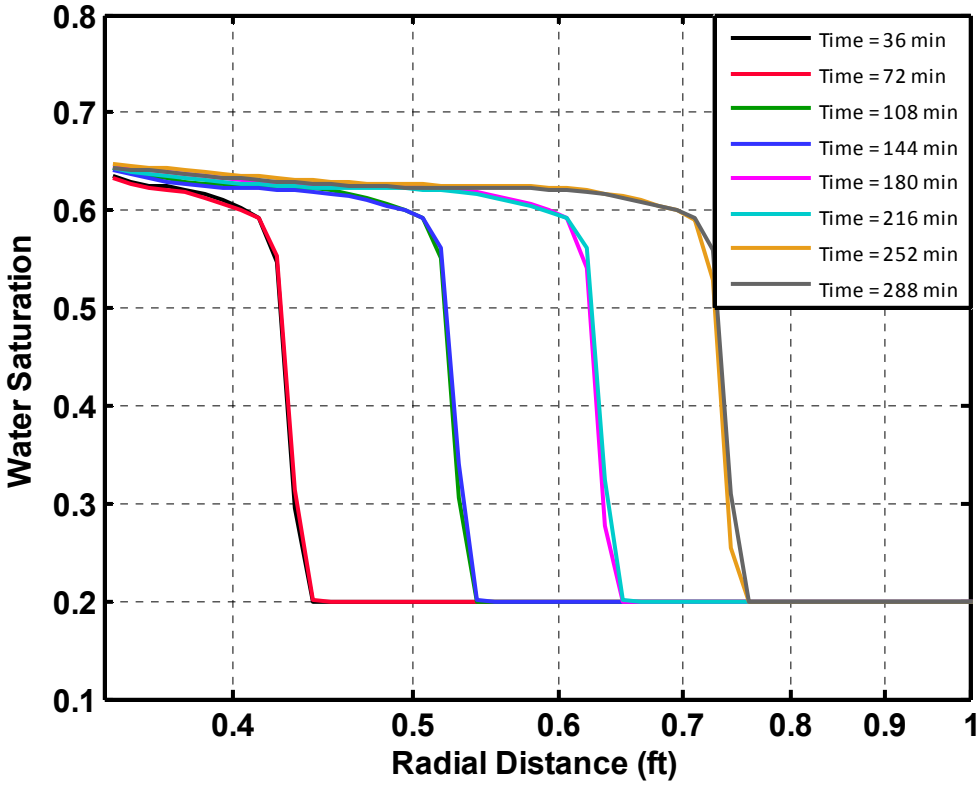

Figure 4-10: Radial profile of water saturation at the end of injection and shut-in times. In this case study, formation permeability is equal to 0.01 mD.

4.4.2 Formation with 0.1 mD Permeability

In this section, I present the validation of the baseline/calibration method using a numerical reservoir model with a formation permeability of 0.1 mD. Reservoir and fluid properties are those described in **Chapter 3**. For the simulation of this case study of the B/C test, I considered injection of water in 4 different stages as shown in **Figure 4-11**. **Figure 4-12** shows time variation of bottom-hole pressures and cumulative injected water values.

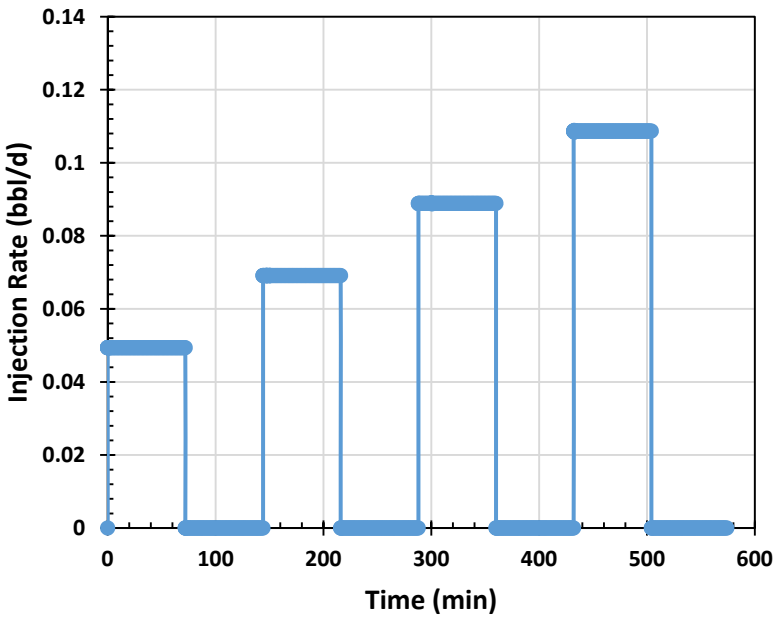

Figure 4-11 : Time variation of water injection rate for a B/C test when performed for a formation with a permeability equal to 0.1 mD.

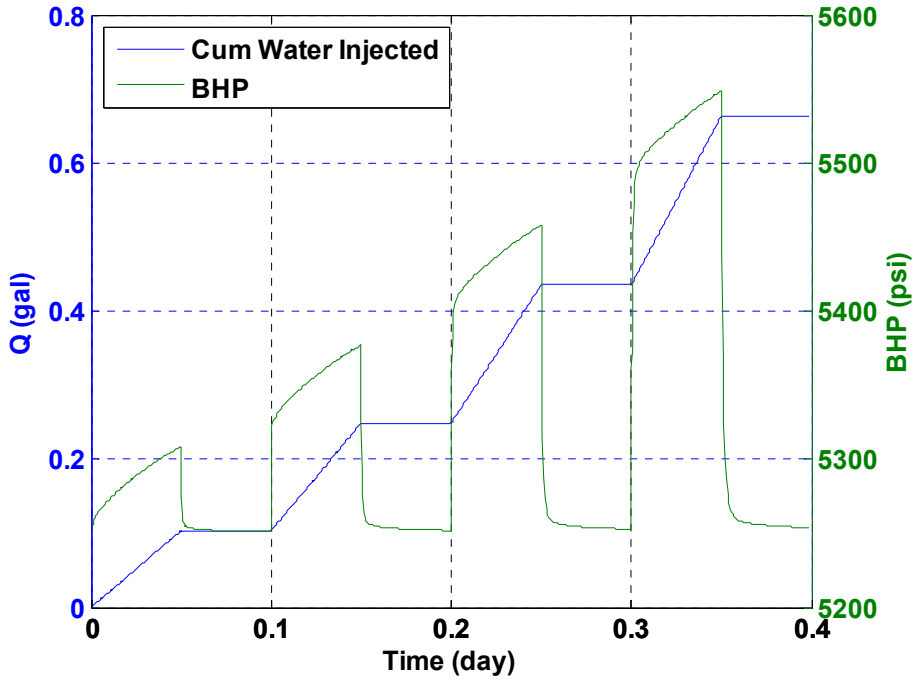

Figure 4-12: Numerical simulation output for a case study with gas and water phases. Formation permeability is assumed to be 0.1mD. This figure shows cumulative injected water and bottom-hole pressure (BHP) versus time.

Similar to **Section 4.4.1**, I plotted a graph of $ln\left(\frac{r_e}{r_w}\right)$ versus $\frac{p_i - p_{wf}}{q}$ in order to estimate alignment pressure for each pair. **Figure 4-13** shows B/C trends alignment for first, second, and third pairs. **Table 4-2** summarizes matching reservoir pressures, cumulative injected water, and average slope for each pair of B/C trends at alignment.

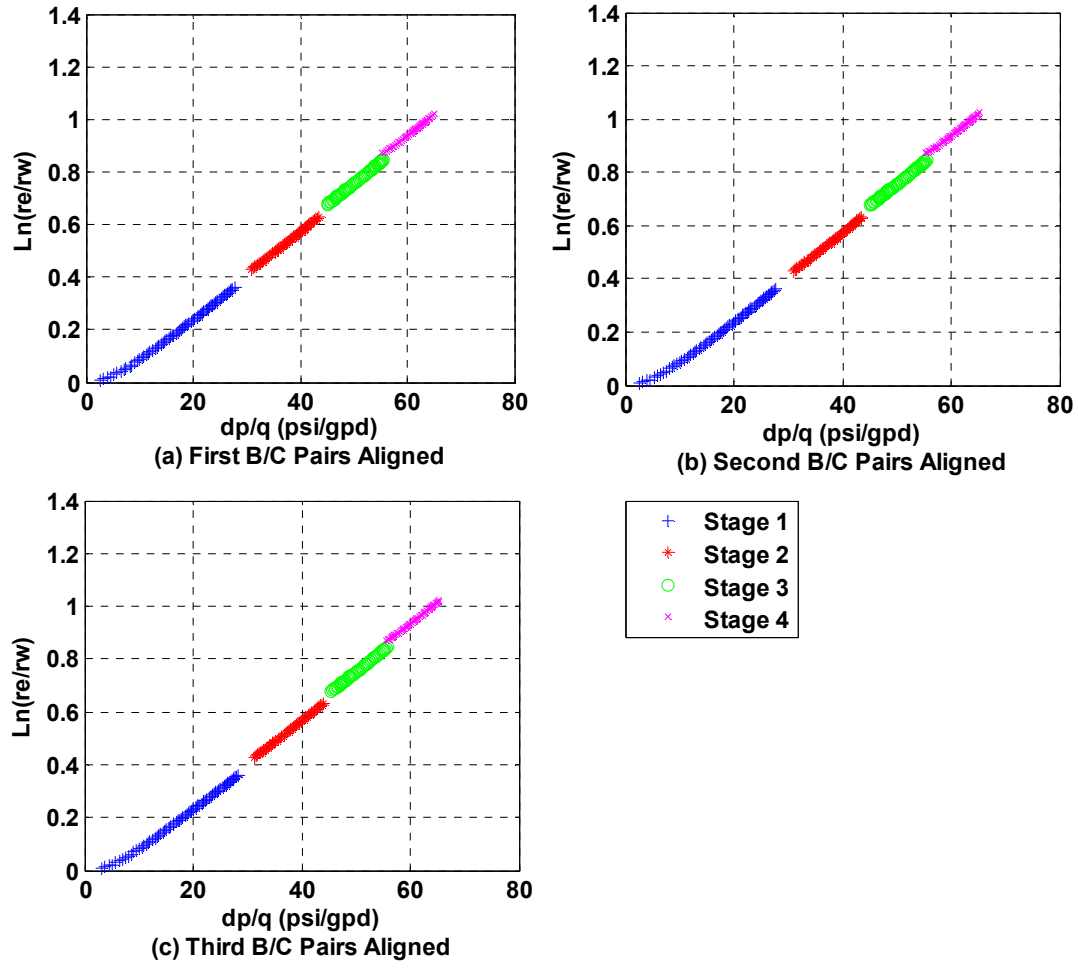

Figure 4-13: Baseline/calibration alignment for a reservoir with 0.1 mD permeability. (a) First B/C pair is aligned at 5251 psi, (b) second B/C pair is aligned at 5252 psi, and (c) third B/C pair is aligned at 5253 psi.

Table 4-2: Summary of cumulative injected water, reservoir pressure match, and average slope for each pair of baseline/calibration trends. In this simulation, formation permeability is assumed to 0.1 mD.

Pair	Q (gal)	P_r-match (psi)	Slope (Gpd/psi)
1	0.104	5251.5	0.015
2	0.249	5252	0.0166
3	0.436	5253.2	0.016

Similar to **Section 4.4.1**, the baseline/calibration supercharging was corrected by plotting calibrated baseline reservoir pressures versus cumulative injected water. A linear trend line was drawn through matching pressure points, and was extrapolated to zero cumulative water injection. Final estimation of reservoir pressure is the pressure at zero cumulative injected water. In this numerical case study, final estimate of reservoir pressure is 5250.9 psi with 0.017% error as shown in **Figure 4-14**.

It is observed that the percentage of error in this case study is lower in comparison with the case study with permeability equal to 0.01 mD. This error is due to the supercharging phenomena which is higher in lower permeability reservoirs. Therefore the percentage of error is higher in the case study with lower permeability.

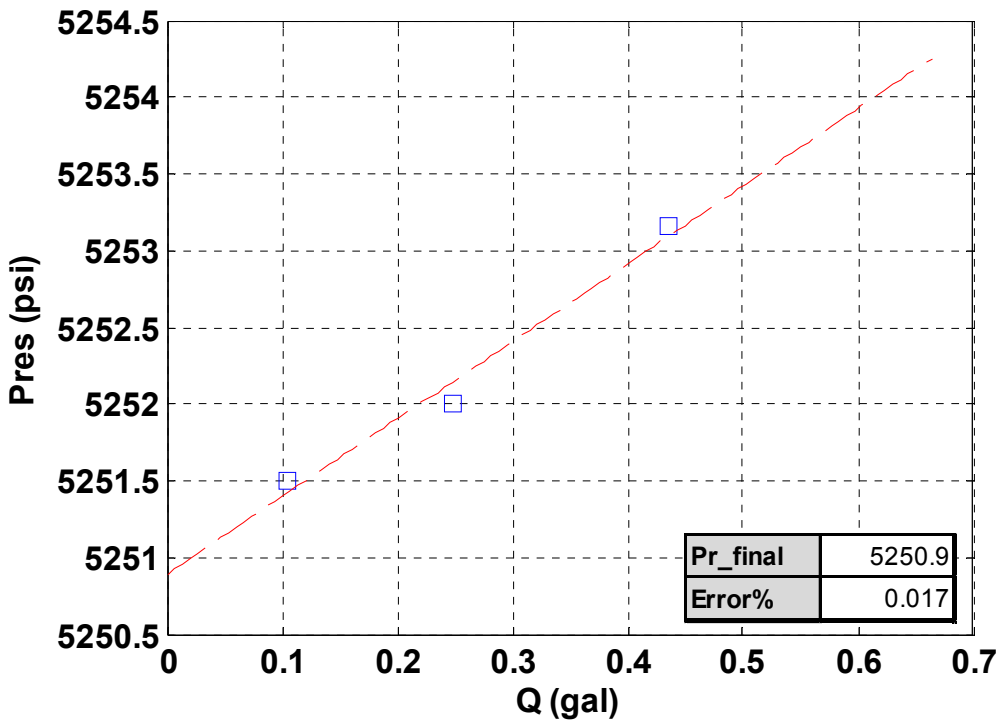

Figure 4-14: Baseline/calibration supercharging correction for reservoir simulation with permeability 0.1 mD. A linear trend line was drawn through pressure match points and extrapolated to zero cumulative water injected. R^2 for the linear trend line is 0.97. The final estimate of reservoir pressure is 5250.9 psi.

Figure 4-15 compares the alignment matching pressure with calculated average pressure of invaded zone. Alignment pressures agree well with calculated average pressures at the end of each shut-in time. In this figure alignment pressures are shown as blue points. **Figure 4-16** shows the agreement between average pressures of invaded area and alignment B/C pressures as a function of time.

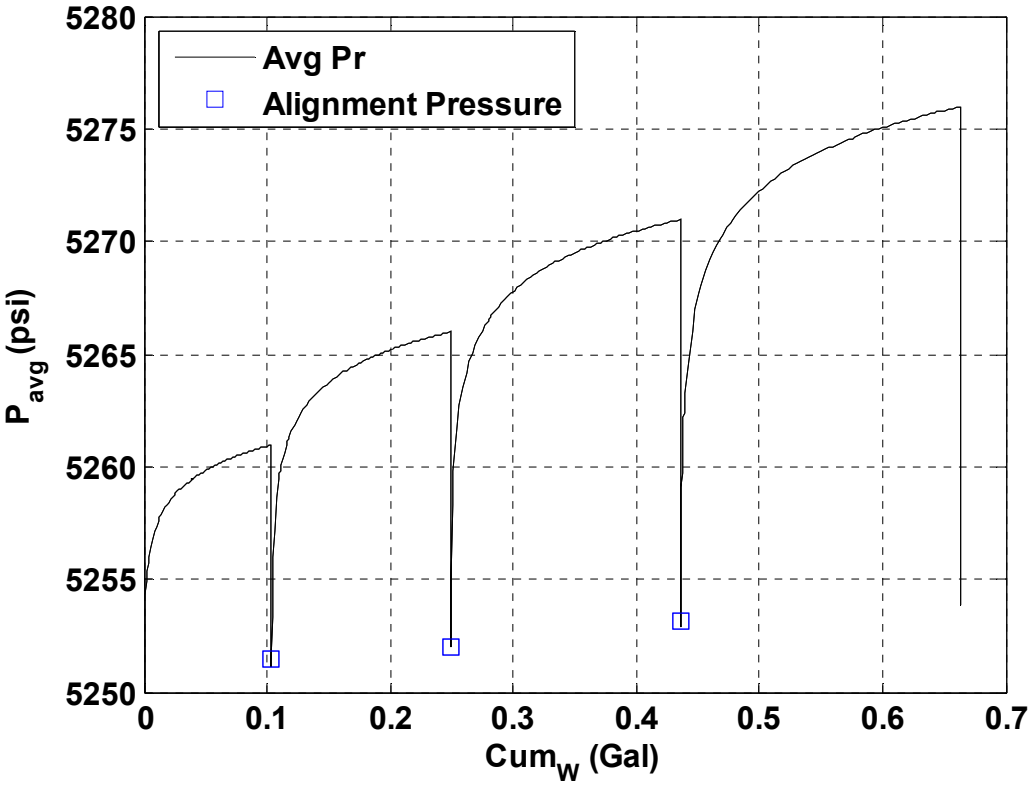

Figure 4-15: Average pressures of invaded zone versus cumulative injected water for a numerical simulation with permeability equal to 0.1 mD. Alignment Pressures have good agreement with average reservoir pressures at the end of shut-in times.

The maximum value of effective water permeability for this simulation model is 0.03. Using Equation (2-62), calculated effective water permeability is 0.025 mD which represents the average effective permeability to water in the radius of invasion. Using the rock-fluid properties, described in **Figure 3-6**, I estimated gas effective permeability as

$$k_{eg} = \frac{0.8}{0.3} * 0.025 = 0.067\, mD.$$

Figure 4-17 shows water saturation distribution at the end of injection and shut-in times.

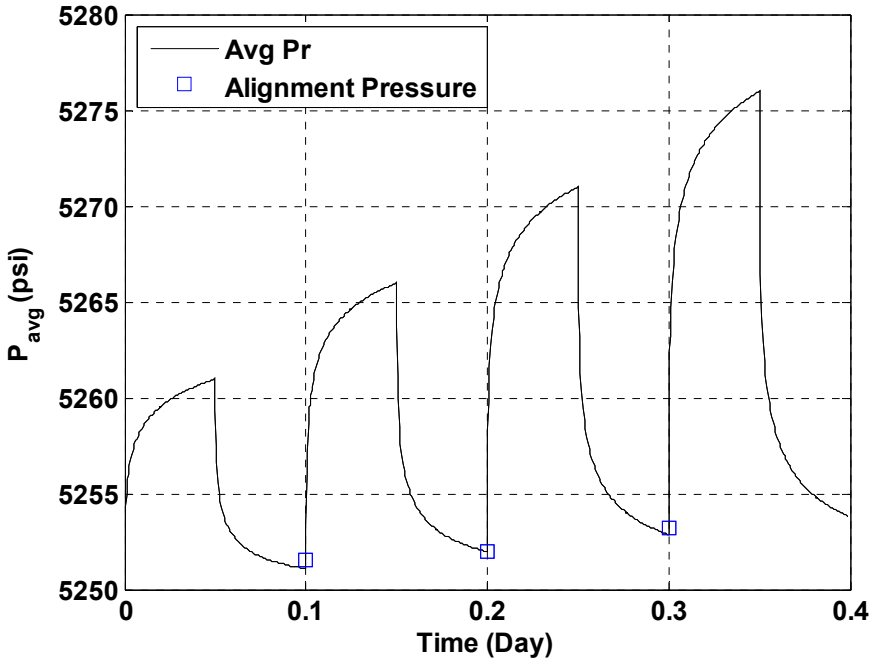

Figure 4-16: Average pressures versus time for a numerical simulation with permeability 0.1 mD. Alignment pressures are approximately the same as average pressure of invaded zone at the end of shut-in times.

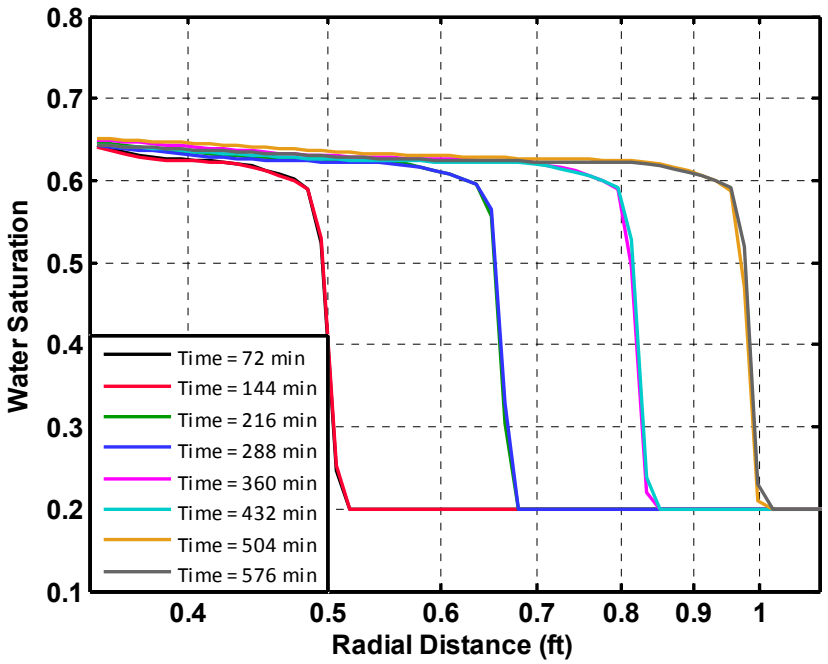

Figure 4-17: Radial profile of water saturation at the end of injection and shut-in times. In this case study, formation permeability is equal to 0.1 mD.

4.4.3 Formation with 0.001 mD Permeability

In this section, I present the validation of the baseline/calibration method in a numerical reservoir model with a formation permeability of 0.001 mD. Reservoir and fluid properties are those described in **Chapter 3**. For the simulation of this case study of B/C test, I injected of water in 4 discrete stages as shown in **Figure 4-18**. **Figure 4-19** shows the schedule of bottom-hole pressure and cumulative injected water. As shown in this figure, I used lower injection rates because formation permeability of this numerical simulation was very low, and high injection rates might propagate a fracture.

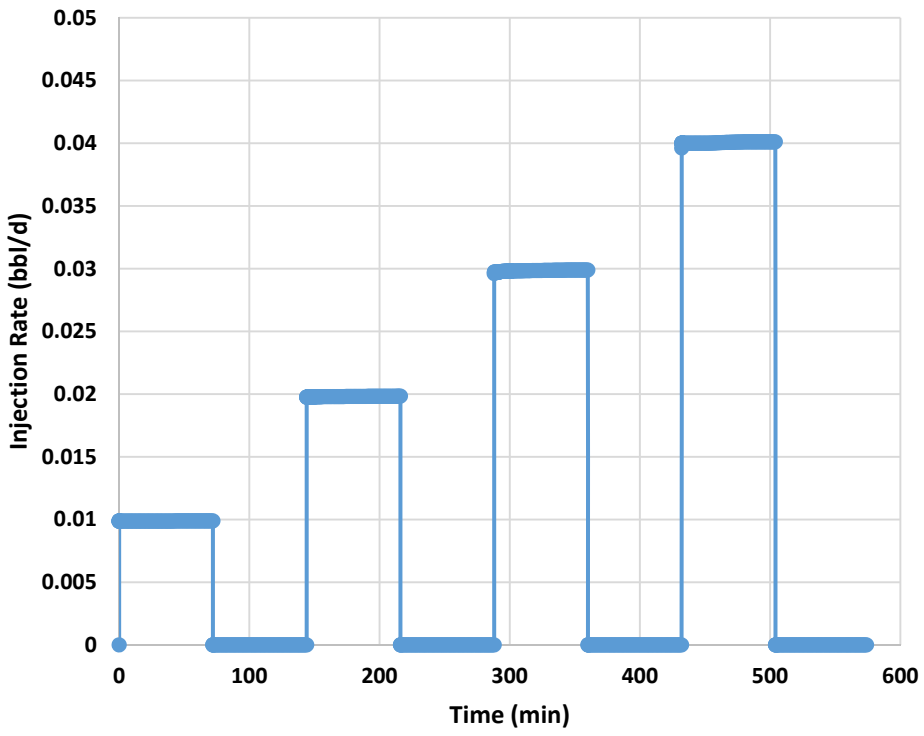

Figure 4-18 : Time variation of injection rate for B/C test when performed for a formation with permeability equal to 0.001 mD.

Similar to **Section 4.4.1**, I plotted a graph of $ln\left(\frac{r_e}{r_w}\right)$ versus $\frac{p_i - p_{wf}}{q}$ to estimate alignment pressures for each pair of B/C trends. **Figure 4-19** presents B/C trends alignment for the first, second, and third pairs. **Table 4-3** summarizes matching reservoir pressures, cumulative injected water, and average slope for each pair of B/C trends at alignment.

As described in **Section 4.4.1**, baseline/calibration supercharging is corrected by plotting calibrated baseline reservoir pressures versus cumulative injected water. I passed a linear trend line through alignment pressure points, and extrapolated it to zero cumulative injected water. Final estimated reservoir pressure is the pressure at zero cumulative injected water where reservoir is at the initial condition. In this numerical case study, the final estimate of reservoir pressure is 5260 psi with 0.19% error as shown in **Figure 4-21**.

It is observed that the percentage of error in this case in higher than that in other cases. Since in this numerical simulation model, the assumed formation permeability is lower than the previous two cases, the supercharging effect is has higher impact in calculating initial reservoir pressure, and consequently, the error is higher in this case study. However, the error of 0.19% is still very low, and less than 1%.

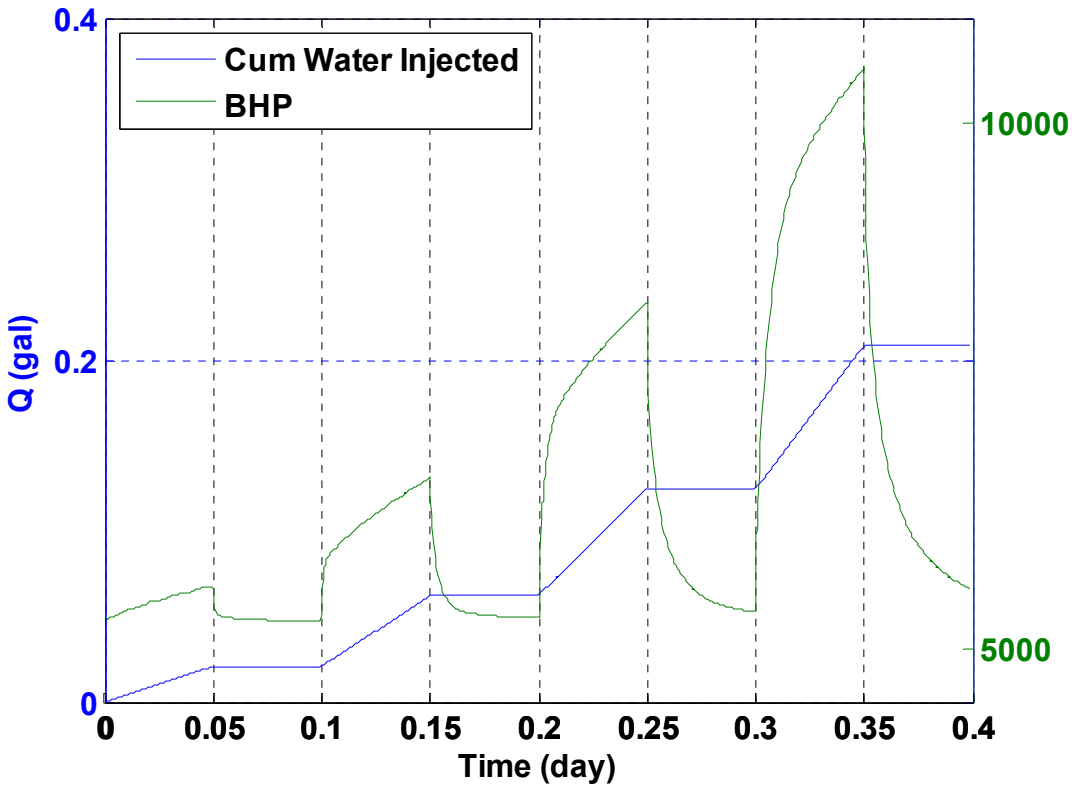

Figure 4-19: Numerical simulation output for a reservoir with two phases of gas and water. Formation permeability is assumed to be 0.001mD. This figure shows cumulative water injected and bottom-hole pressure (BHP) versus time.

Figure 4-22 compares the alignment pressures with calculated average pressures within the radius of invasion. Alignment pressures agree well with calculated average pressures at the end of each shut-in time. **Figure 4-23** shows the agreement between average pressures and alignment B/C pressures as a function of time.

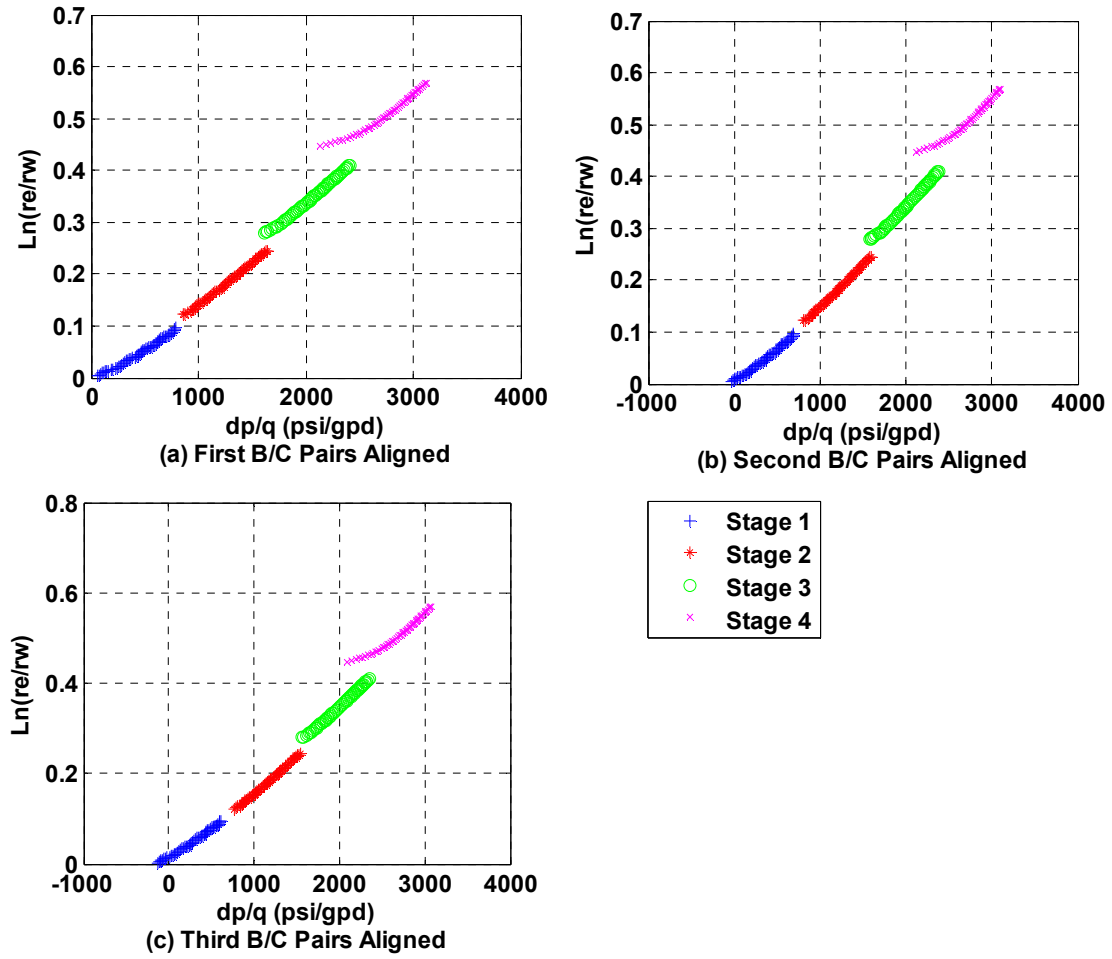

Figure 4-20: Baseline/calibration alignment for a case study with 0.001 mD permeability. (a) First B/C pair is aligned at 5271 psi, (b) second B/C pair is aligned at 5311 psi, and (c) third B/C pair is aligned at 5347 psi.

Table 4-3: Summary of cumulative injected water, reservoir pressure match, and average slope for each pair of baseline/calibration trends. In this simulation, formation permeability is assumed to 0.001 mD.

Pair	Q (gal)	P_r-match (psi)	Slope (Gpd/psi)
1	0.021	5271	0.00014
2	0.062	5311	0.00016
3	0.125	5347.3	0.00015

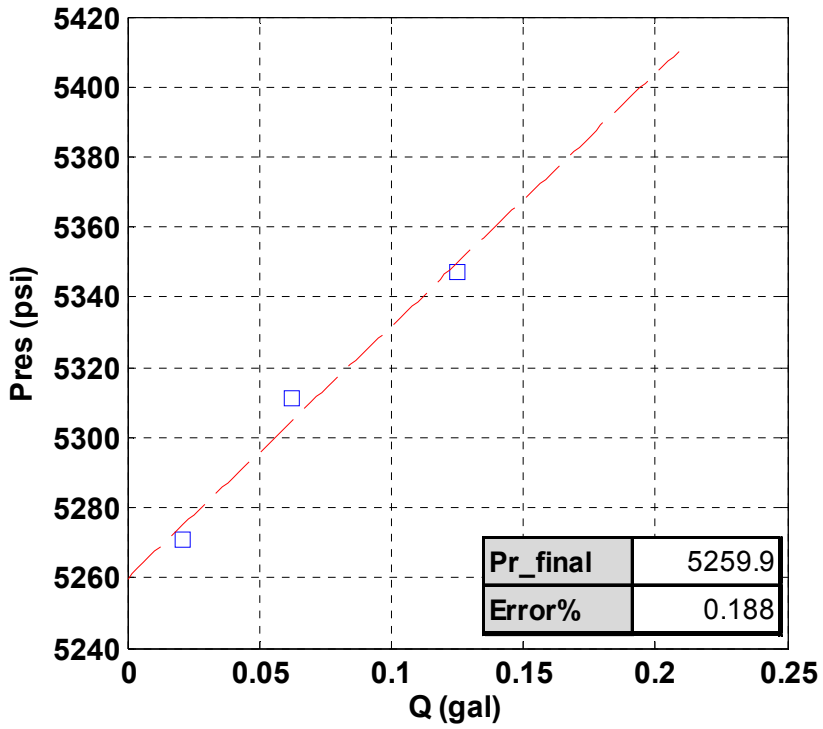

Figure 4-21: Baseline/calibration supercharging correction for reservoir simulation with permeability 0.001 mD. The linear trend line passes through pressure match points and extrapolated to zero cumulative water injected. R^2 of the linear trend line is 0.98. The final estimate of reservoir pressure is 5259.9psi.

Using Equation (2-62), calculated effective water permeability is 0.00024 mD. The maximum value of effective water permeability for this numerical simulation model is 0.0003 mD. Calculated permeability of 0.00024 mD represents the average effective permeability to water through the radius of invasion. Using the rock-fluid properties, in **Figure 3-6**, I estimated gas effective permeability as

$$k_{eg} = \frac{0.8}{0.3} * 0.00024 = 0.00064\, mD.$$

Figure 4-24 shows water saturation distribution at the end of injection and shut-in times.

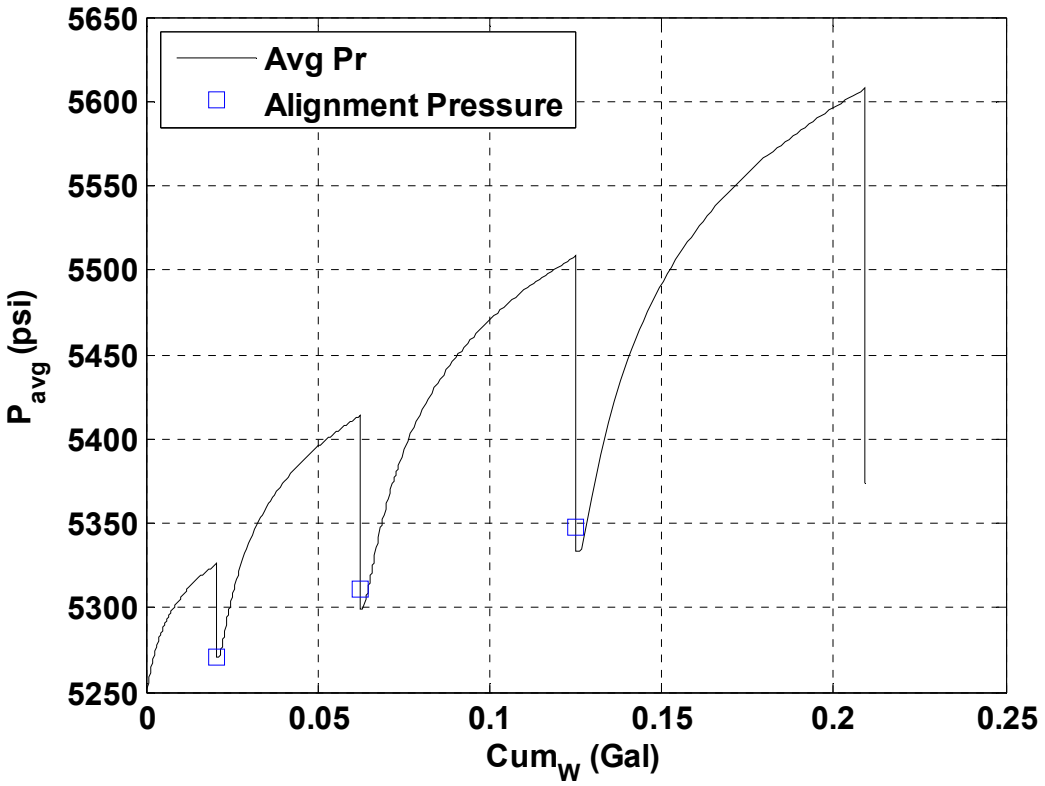

Figure 4-22: Average pressures of invaded zone versus cumulative water injected for a numerical simulation with permeability 0.001 mD. The alignment pressures are approximately the same as average pressures at the end of shut-in times.

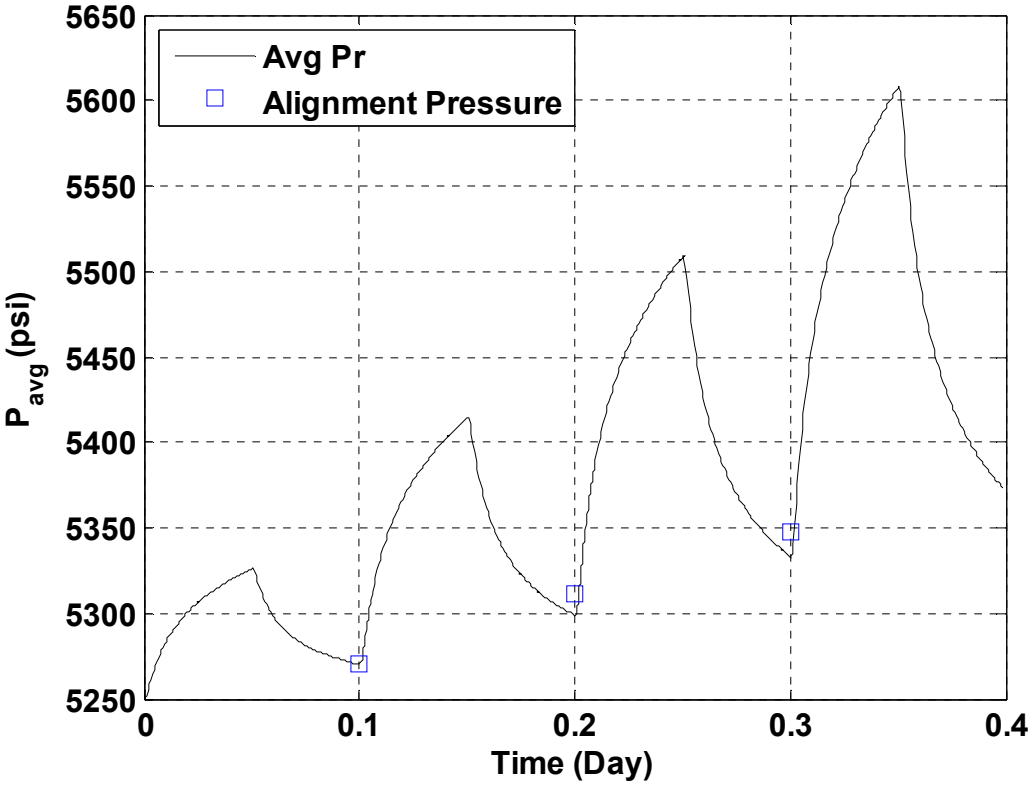

Figure 4-23: Average pressures of invaded area versus time for a numerical simulation with permeability 0.001 mD. Alignment pressures are approximately the same as average pressures at the end of shut-in times.

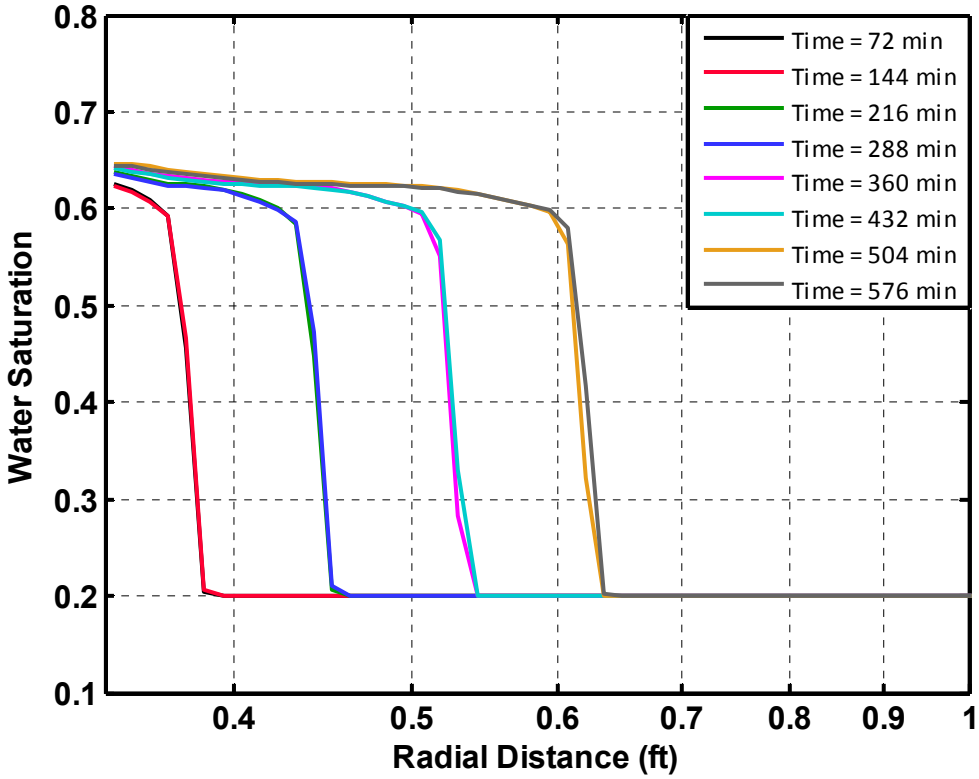

Figure 4-24: Radial profile of water saturation at the end of injection and shut-in times. In this case study, formation permeability is equal to 0.001 mD.

Chapter 5

Field Trial Applications

5.1 Introduction

Baseline/calibration technique has been tested on several wells in the Almond formation of Wamsutter field, Wyoming. These wells are operated and B/C tests were performed by BP. In two of the wells studied, downhole gauges were used to measure sandface pressure and flow rate with high quality. Using downhole gauges in these two wells provided the opportunity to investigate the difference between surface and downhole pressures. The effect of gas influx, pressure gradient, and frictional pressure drop were calculated for conversion of pressure and injection rate from surface to sandface condition. In this study, I used the sandface pressure and injection rate data provided by BP unconventional gas flagship. The operator has converted surface flow rate and pressure to those in sandface condition.

The most practical and operational cost effective protocol for a B/C test is Falling Fluid Level Test (FFLT[1]) protocol. Through a FFLT, it is possible to use surface gauges and therefore performing B/C test becomes more cost effective. FFLT is BP's desirable protocol to conduct a B/C test. However, BP has also tested the B/C method using Constant Pressure Injection Test (CPIT[2]) and

[1] FFLT consists of injection by changing sandface rate and pressure at the same time.
[2] CPIT consists of injection at a constant bottom-hole pressure followed by a short shut-in time.

Constant Rate Injection Test (CRIT[3]) protocols. Performing a B/C test using a CPIT or CRIT protocol is less practical and more expensive in comparison to FFLT due to the need for a separate and special system to keep the sandface pressure or injection rate constant. BP has tested B/C method using CPIT and CRIT less frequently and FFLT more frequently.

In this chapter, I evaluated sandface pressure and injection rate data obtained from B/C tests, performed on two Wamsutter wells. I estimated reservoir pressure value using the method described in **Chapter** 2.

5.2 Field Trial One

In this field trial, baseline/calibration test is performed using a FFLT. Water was injected in 4 different injection stages as shown in **Figure 5-1**. In this field trial, water was injected for approximately 30 minutes in each stage followed by 2 minutes shut-in. **Figure 5-2** demonstrates the time variation of sandface pressure and cumulative injected water.

During early stages of completion, when a B/C test is conducted, information such as porosity, initial water saturation, residual gas saturation, and reservoir height are not available. According to Equation (2-51),

$$r_e = \sqrt{\frac{5.615\ Q}{\phi\pi h\left(1 - S_{wi} - S_{gr}\right)} + r_w^2}\ . \qquad (2\text{-}51)$$

Assuming constant height, porosity, initial water saturation, and residual gas saturation, then $\ln(Q)$ is proportional to $ln\left(\frac{r_e}{r_w}\right)$. Therefore, a graph of

[3] CRIT consists of injection at a constant flow rate while bottom-hole pressure is variable.

$\ln(Q)$ versus $\Delta p/q$ can be used to find alignment pressure for each injection pair. **Figure 5-3** shows B/C trend alignment between different stages of the test trial.

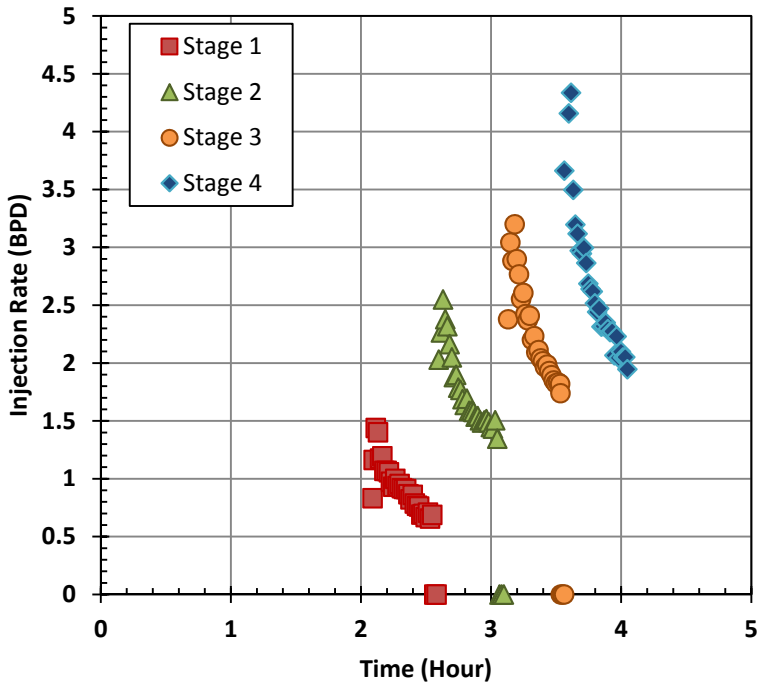

Figure 5-1: Time variation of injection rate during baseline/calibration field trial one. This test was conducted with FFLT protocol.

Table 5-1 summarizes the alignment reservoir pressures and cumulative injected water for each B/C pair. **Figure 5-4** shows that supercharging correction is applied to find final estimate of reservoir pressure as 4585 psi.

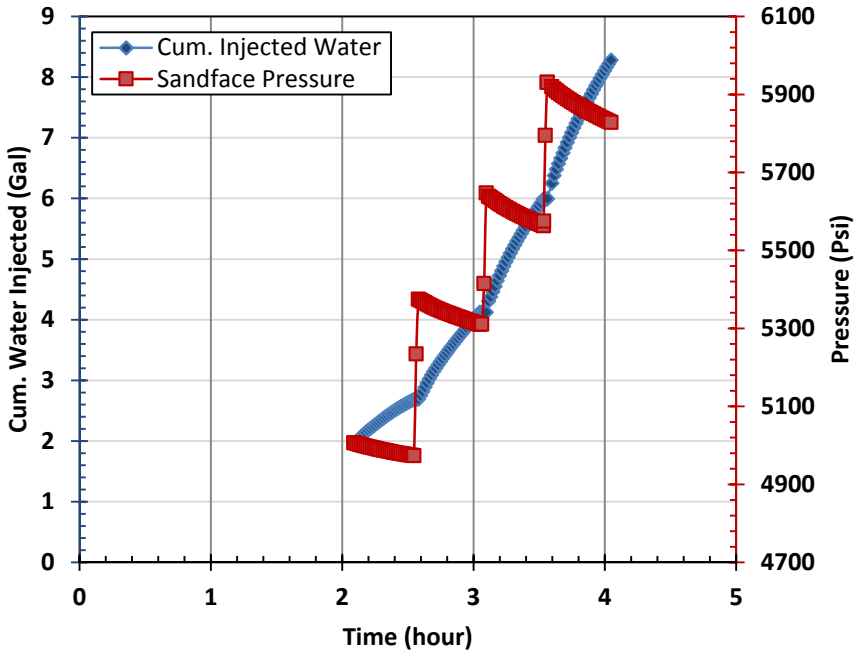

Figure 5-2: Cumulated injected water and sandface pressure during baseline/calibration field trial one.

Table 5-1: Summary of cumulative injected water and alignment reservoir pressure for each baseline/calibration trend, field trial one.

Pair	Q (gal)	P_r-match (psi)
1	2.692	4850
2	4.127	5050
3	5.991	5200

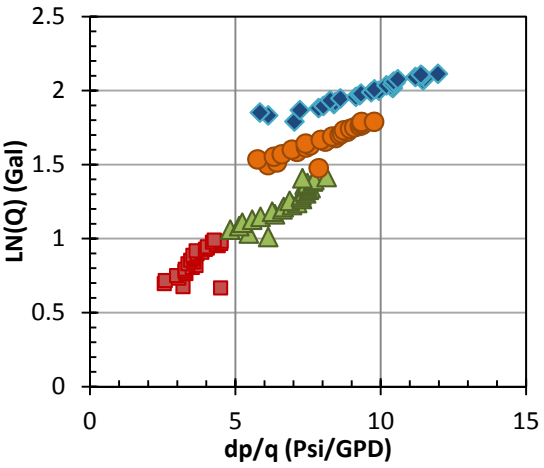

(a) Stage one and stage two of trend lines are aligned at pressure equal to 4850 psi.

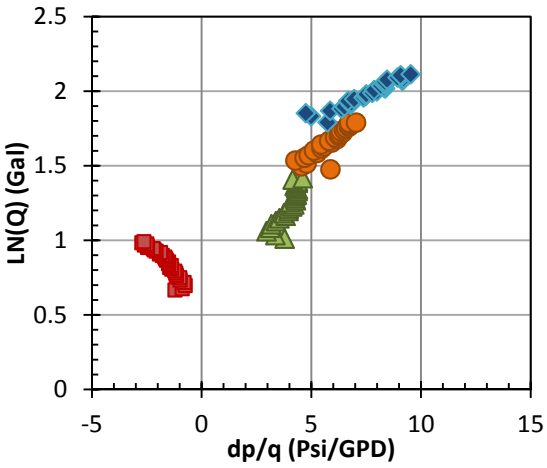

(b) Stage two and stage three of trend lines are aligned at pressure equal to 5050 psi.

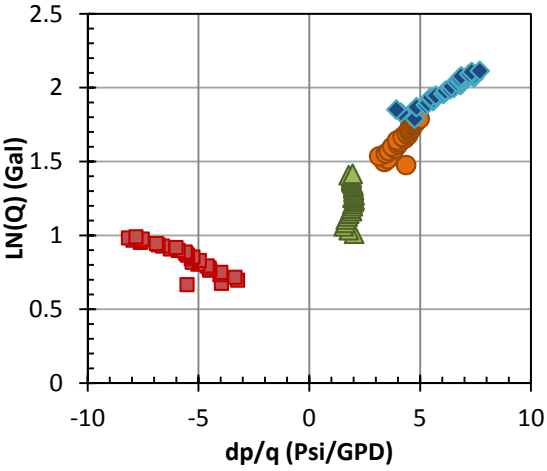

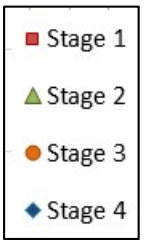

(c) Stage three and stage four of trend lines are aligned at pressure equal to 5200 psi.

Figure 5-3: Baseline/calibration trend alignment for the field trial one. (a) First pair is aligned at $4850\ psi$, (b) second pair is aligned at $5050\ psi$, and (c) third pair is aligned at $5200\ psi$.

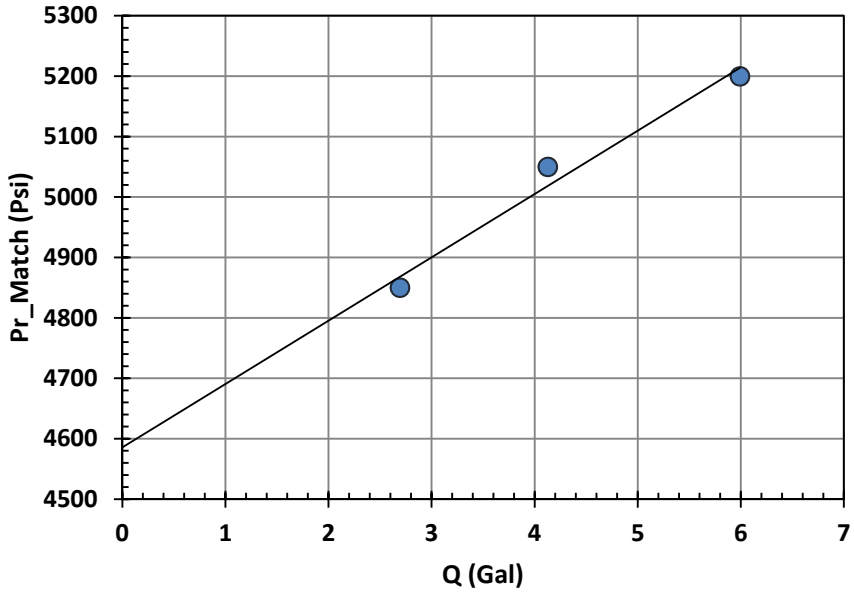

Figure 5-4: Supercharging correction for baseline/calibration field trial one. A linear trend line passes through pressure points and extrapolates to zero cumulative water injected. R^2 for this linear trend line is 0.97.

5.3 Field Trial Two

In this section, I analyzed the pressure and injection rate data from another baseline/calibration field trial performed with a FFLT protocol. Water was injected in 4 discrete stages as shown in **Figure 5-5**. Each injection stage lasted approximately 15 minutes followed by 3 minutes of shut-in. **Figure 5-6** presents the schedule of sandface pressures and cumulative injected water values.

Figure 5-7 shows B/C trend alignment between different stages of the test trial. Alignment pressures and cumulative injected water for each pair are summarized in **Table 5-2**.

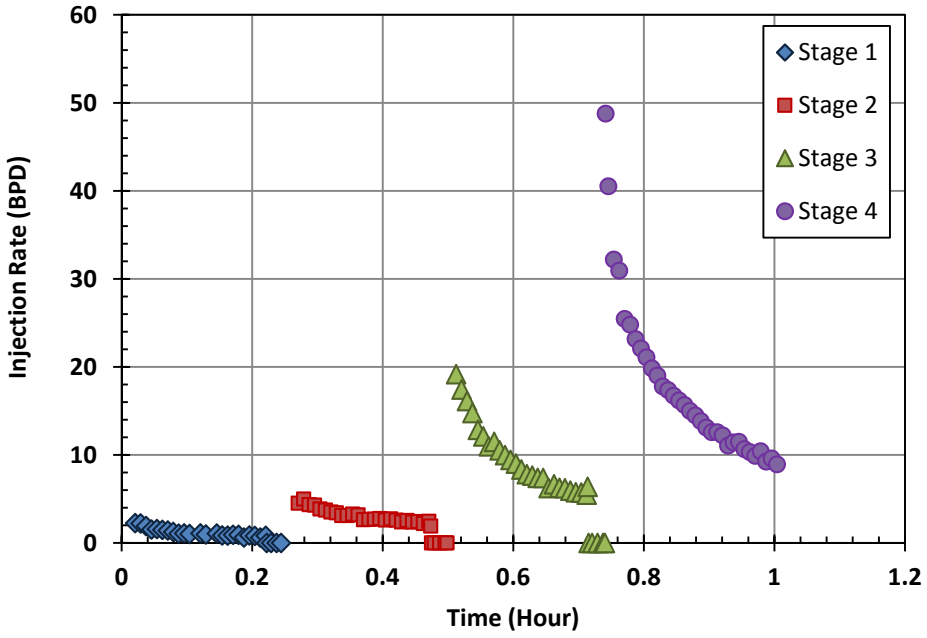

Figure 5-5: Time variation of injection rate during baseline/calibration field trial two. This test was conducted with FFLT protocol.

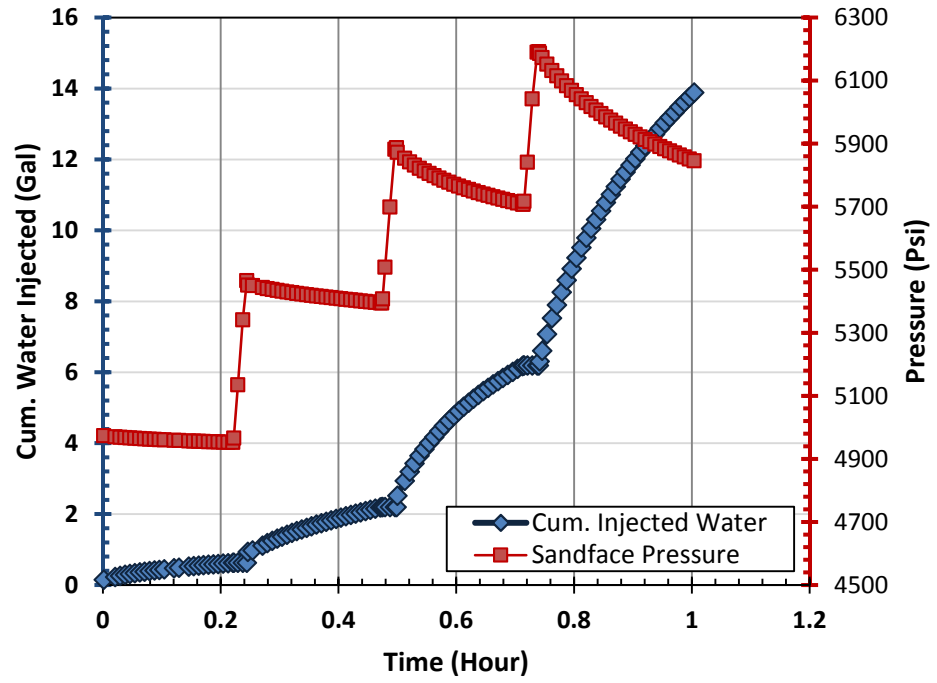

Figure 5-6: Cumulated injected water and sandface pressure during baseline/calibration field trial two.

The supercharge correction was applied to determine the final estimate of reservoir pressure as shown in **Figure 5-8**. Reservoir pressure was calculated to be 4930 psi in this field trial.

Table 5-2: Summary of cumulative injected water and alignment reservoir pressure for each baseline/calibration trend, field trial two.

Pair	Q (gal)	P_r-match (psi)
1	0.632	4900
2	2.203	5325
3	6.195	5600

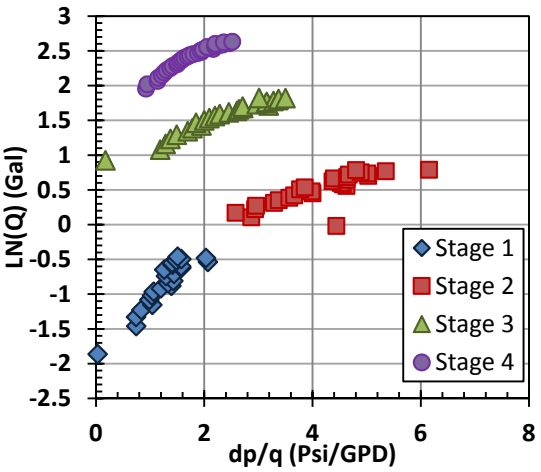

(a) Stage one and stage two of trend lines are aligned at pressure equal to 4900 psi.

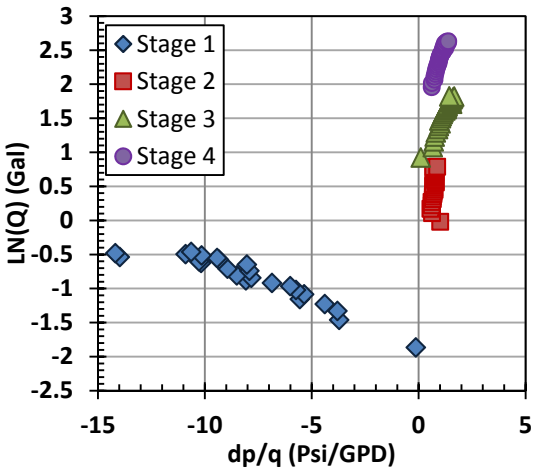

(b) Stage two and stage three of trend lines are aligned at pressure equal to 5325 psi.

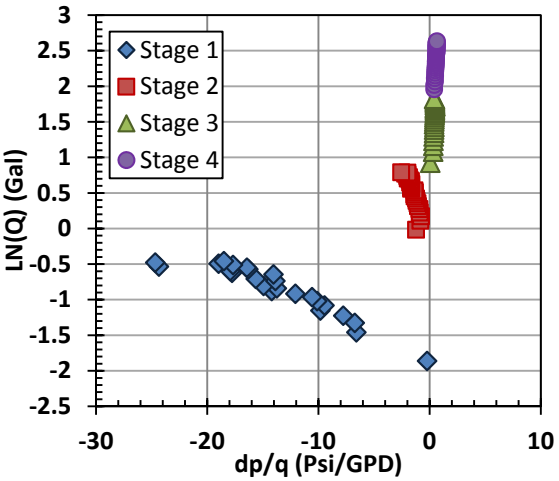

(c) Stage three and stage four of trend lines are aligned at pressure equal to 5600 psi.

Figure 5-7: Baseline/calibration trend alignment for the field trial two. (a) First pair is aligned at $4900\ psi$, (b) second pair is aligned at $5325\ psi$, and (c) third pair is aligned at $5600\ psi$.

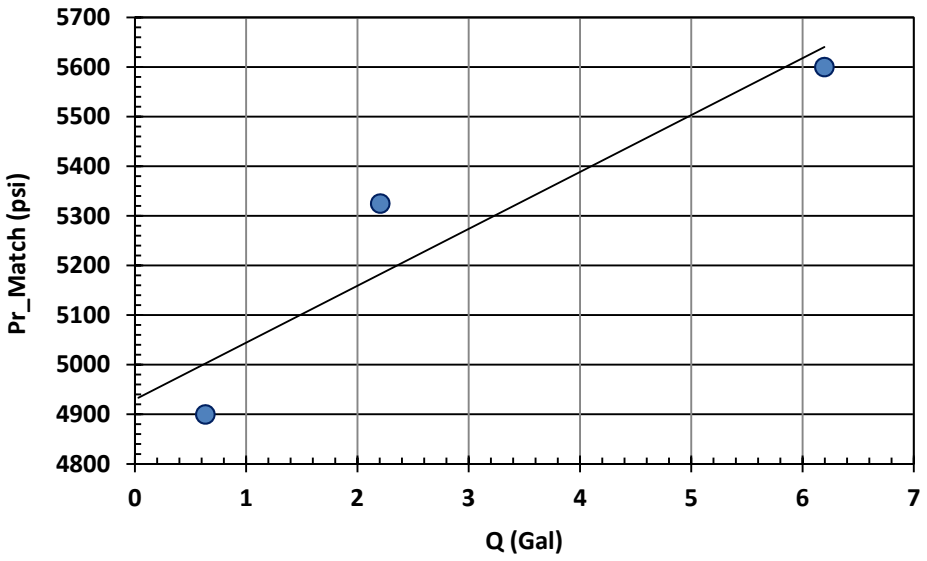

Figure 5-8: Supercharge correction for baseline/calibration field trial two. A linear trend line passes through pressure points and extrapolates to zero cumulative water injected. R^2 for this linear trend line is 0.87.

Chapter 6

Summary and Conclusions

I developed the mathematical basis for a new and operationally cost effective approach, called baseline/calibration, to estimate formation pressure and effective water permeability. I derived and successfully validated mathematical formulations for pressure variations during a baseline/calibration test. These mathematical formulations were based on (i) the line-source solution to the diffusivity equation, (ii) the principle of superposition in time, and (iii) the approximately piston-like displacement of injected water. The derived mathematical formulation verified that each pair of trends should be aligned linearly at a specific pressure. The alignment pressure for each pair was found to be the average pressure of invaded area at the onset of corresponding injection stage. I presented a method to correct for supercharging effect and determined final estimated reservoir pressure.

I constructed several numerical reservoir simulation models to validate baseline/calibration technique. These models included different representative petrophysical rock types for tight gas sand formations of Wamsutter field. Using the baseline/calibration method, initial reservoir pressure was estimated accurately for all numerical simulation models. The range of error in calculated reservoir pressure for these models was from 0.017% to 0.188%. I observed that the percentage of error was higher in formations with lower permeability.

Accuracy of pressure estimates was reduced in tight formations due to a more significant supercharging.

I developed and validated a new approach to estimate effective permeability to water. Simulation results showed calculated effective water permeability agreed well with actual effective water permeability.

The results of numerical simulations and field trials showed that the baseline/calibration method can be successful in estimating formation pressure in very short test times.

References

Abdollah-Pour, R. 2011. Development and Application of a 3D Equation-of-State Compositional Fluid-Flow Simulator in Cylindrical Coordinates for Near-Wellbore Phenomena. Ph.D., University of Texas at Austin, Texas, USA.

Adams, J.R., Dotson, B., Sebastian, H., and Motealleh, S. 2013. Baseline/Calibration Method for Reservoir Pressure Determination. Presented at the SPE Unconventional Resources Technology Conference, Denver, Colorado, 12-14 August, SPE-168900-MS. http://dx.doi.org/10.1190/URTEC2013-022.

Adams, J.R., Motealleh, S., Sebastian, H., Jiang, Y., and Dotson, B. 2012. Method of Determining Reservoir Pressure. USA Patent No.

Agarwal, R.G., Al-Hussainy, R., and Ramey Jr., H.J. 1965. The Importance of Water Influx in Gas Reservoirs. *Journal of Petroleum Technology* **17** (11): 1336-1342. SPE-1244-PA. http://dx.doi.org/10.2118/1244-PA.

Cramer, D.D. and Nguyen, D.H. 2013. Diagnostic Fracture Injection Testing Tactics in Unconventional Reservoirs. Presented at the SPE Hydraulic Fracturing Technology Conference, The Woodlands, Texas, 4-6 February, SPE-163863-MS. http://dx.doi.org/10.2118/163863-MS.

Economides, M.J., Hill, A.D., Economides, C.E., and Zhu, D. . 2013. *Petroleum Production Systems*, second edition. Westford, Masscachusetts: Pearson Education.

Geffen, T.M., Parrish, D.R., Haynes, G.W., and Morse, R.A. 1952. Efficiency of Gas Displacement From Porous Media by Liquid Flooding. *Journal of Petroleum Technology* **4** (02): 29-38. SPE-952029-G. http://dx.doi.org/10.2118/952029-G.

Jin, M., Zhang, W., and Zhang, H. 2013. Integrated Well Test Strategy in Unconventional Tight Gas Reservoirs-Learning and Experiences from an Actual Field Project. Presented at the International Petroleum Technology Conference, Beijing, China, 26-28 March, IPTC-16950-Abstract. http://dx.doi.org/10.2523/16950-ABSTRACT.

Lee, J., Rollins, J.B., and Spivey, J.P. 2003. *Pressure Transient Testing*, first edition. Richardson, Texas: Society of Petroleum Engineers.

Martin, A.R., Cramer, D.D., Nunez, N., and Roberts, N.R. 2013. A Method to Perform Multiple Diagnostic Fracture Injection Tests Simultaneously in a Single Wellbore. *SPE Production & Operations* **28** (02): 91-200. SPE-152019-PA. http://dx.doi.org/10.2118/152019-PA.

Martin, J.C. 1959. The Simplified Equations of Flow in Gas Drive Reservoirs and the Theoretical Foundation of Multiphase Pressure Buildup Analyses. *Society of Petroleum Engineers* **216**. SPE 1235-G.

Matthews, C.S. and Russell, D.G. 1967. *Pressure Buildup and Flow Tests in Wells*, first edition. Dallas, Texas: Society of Petroleum Engineers.

Merletti, G.D., Abdollah-Pour, R., and Spain, D.R. 2013. Calibration of Static Reservoir Models with Dynamic Data for Efficient Tight-Gas Field Development (Wyoming, US). Presented at the SPE Unconventional Gas Conference and Exhibition,, Muscat, Oman, 28-30 January, SPE-164031-MS. http://dx.doi.org/10.2118/164031-MS.

Peters, E.J. 2012. *Advanced Petrophysics*, first edition, Vol. 2. Austin, Texas: Live Oak Book Company.

Satter, A., Igbal, G.M., and Buchwalter, J.L. 2008. *Practical Enhanced Reservoir Engineering*, first edition. Tulsa, Oklahoma: PennWell Corporation.

Soliman, M. Y. and Kabir, C. S. 2012. Testing Unconventional Formations. *Journal of Petroleum Science and Engineering* **92-93**: 102-109. http://dx.doi.org/10.1016/j.petrol.2012.04.027.

Soliman, M.Y. 1986. Analysis of Buildup Tests With Short Producing Time. *SPE Formation Evaluation* **1** (04): 363-371. SPE-11083-PA. http://dx.doi.org/10.2118/11083-PA.

Soliman, M.Y., Craig, D., Bartko, K., Rahim, Z., Ansah, J., and Adams, D. 2005. New Method for Determination of Formation Permeability, Reservoir Pressure, and Fracture Properties from a Minifrac Test Presented at the 40th U.S. Symposium on Rock Mechanics (USRMS), Anchorage, Alaska, 25-29 June, ARMA-05-658.

Soliman, M.Y., Shahri, M., and Lamei, H. 2013. Revisiting the Before Closure Analysis Formulations in Diagnostic Fracturing Injection Test. Presented at the SPE Hydraulic Fracturing Technology Conference, The Woodlands, Texas, 4-6 February, SPE-163869-MS. http://dx.doi.org/10.2118/163869-MS.